

Supporting Information

Ionic Radius-Dependent Self-Assembly of Lanthanide Organic Polyhedra: Structural Diversities and Luminescent Properties

Jing Su^{a,b,c}, Fan Yin^a, Xiao-Fang Duan^a, Jing-Yao Zhou^a, Li-Peng Zhou^a, Chong-Bin Tian^{*a,b,c} and Qing-Fu Sun^{*a,b,c}

a. State Key Laboratory of Structural Chemistry, Fujian Institute of Research on the Structure of Matter, Chinese Academy of Sciences, Fuzhou 350002, P. R. China

b. College of Chemistry and Materials Science, Fujian Normal University, Fuzhou, 350007, China

c. Fujian College, University of Chinese Academy of Sciences, Fuzhou, Fujian, 350002, P. R. China

* Correspondence to: tianchongbin@fjirsm.ac.cn; qfsun@fjirsm.ac.cn

Contents

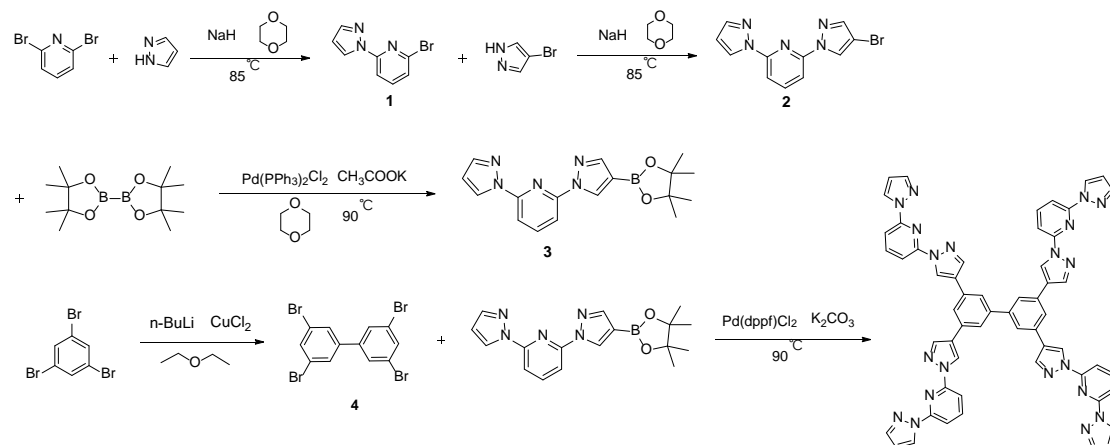
1. General information	S3
2. Synthesis and characterization	S4
2.1 Synthesis and characterization of ligand	S4
2.2 Synthesis and characterization of cages	S8
2.3 ESI-TOF-MS spectra	S22
3. Single crystal X-ray diffraction studies	S33
3.1 Crystal studies	S33
3.2 Volume calculations	S40
4. Host-guest studies	S42
4.1 General procedure for host-guest studies	S42
4.2 Binding constants estimation	S42
5. The rich conformations of the ligand L	S44
6. UV-Vis and FL spectra	S45
7. Reference	S51

1. General information

All chemicals and solvents were purchased from commercial companies and used without further purification unless otherwise stated. Anhydrous solvents were distilled according to standard procedures. Deuterated solvents were purchased from Admas, J&K scientific and Sigma-Aldrich. The 1D and 2D-NMR spectra were measured on Bruker Biospin Avance III (400 MHz) instrument, ^1H -NMR and ^{13}C NMR chemical shifts were referenced to the residual signals of the deuterated solvents used (CDCl_3 , ^1H NMR: $\delta = 7.26$ ppm, ^{13}C NMR: $\delta = 77.0$ ppm; CD_3CN , ^1H NMR: $\delta = 1.94$ ppm, ^{13}C NMR: $\delta = 118.26$ ppm). ESI-TOF-MS spectra of Eu_8L_4 , Sm_6L_3 , Eu_6L_3 and Lu_6L_3 was recorded on Impact II UHR-TOF mass spectrometry from Bruker, while ESI-TOF-MS spectra of other compounds were recorded on LC-QTOF-MS (G6520B), with tuning mix as the internal standard. Data analysis was conducted with the Bruker Data Analysis software (Version 4.3) and simulations were performed with the Bruker Isotope Pattern software and Thermo Xcalibur Qual Browser software (Thermo Foundation 2.0). UV-vis spectra are recorded on UV-2700 UV-vis spectrophotometer from SHIMADZU Corporation. Excitation and emission spectra were recorded on the FS5 spectrofluorometer from Edinburg Photonics. The overall luminescence quantum yields were measured by using the FS5 Spectrometer from Edinburg Photonics (SC-30 Integrating Sphere).

2. Synthesis and characterization

2.1 Synthesis and characterization of ligand.



Scheme S1. Synthetic route of ligand **L**. The preparation of compound **1** and **2** were followed the literature procedure.¹

Synthesis of 2-(1H-pyrazol-1-yl)-6-(4-(4,4,5,5-tetramethyl-1,3,2-dioxaborolan-2-yl)-1H-pyrazol-1-yl)pyridine (**3**):

Compound **2** (1.16 g, 4 mmol, 2 equiv), 4,4,4',4',5,5,5',5'-octamethyl-2,2'-bi(1,3,2-dioxaborolane) (2.54 g, 10 mmol, 5 equiv), CH₃COOK (1.96 g, 20 mmol, 10 equiv) and Pd(PPh₃)₂Cl₂ (140 mg, 0.2 mmol, 0.1 equiv) were dissolved in the anhydrous dioxane solution (20 mL). The reaction mixture was stirred under 90 °C and N₂ atmosphere for 4 h, and then the crude product was purified by column chromatography (SiO₂, DCM/PE, v/v = 3/1) to afford compound **3** as white powder (1 g, 75%). ¹H NMR (400 MHz, CDCl₃, 298 K) δ = 8.81 (s, 1H), 8.53 (m, 1H), 7.96 (m, 1H), 7.85 (7.85 (t, J = 7.9 Hz, 1H)), 7.79 (d, J = 7.7 Hz, 2H), 7.69 (s, 1H), 6.44–6.40 (t, 1H).

Synthesis of 3,3',5,5'-tetrabromo-1,1'-biphenyl (**4**):

1,3,5-tribromobenzene (1.58 g, 5 mmol, 5 equiv) was dissolved in 60 mL anhydrous ether solution which was cooled to -78 °C. After that, n-BuLi (1.2 mL, 3 mmol, 3 equiv) was slowly added into the mixed solution with a constant pressure dropping funnel under N₂ atmosphere, then the reaction mixture was stirred under -78 °C for 4 h. Finally, added CuCl₂ (403 mg, 3 mmol, 3 equiv) to the reaction solution and reacted at

room temperature for 16 hours, while added ammonium chloride aqueous solution to quench n-BuLi. The crude product was treated with a saturated EDTA aqueous solution (100 mL) to remove residual Cu²⁺ ions and then purified by column chromatography (SiO₂, PE) to afford compound **4** as a white powder (1.2 g, 51%). ¹H NMR (400 MHz, CDCl₃, 298 K) δ = 7.69 (t, J = 1.7 Hz, 1H), 7.59 (d, J = 1.7 Hz, 2H).

Synthesis of 3,3',5,5'-tetrakis(1-(6-(1H-pyrazol-1-yl)pyridin-2-yl)-1H-pyrazol-4-yl)-1,1'-biphenyl (L):

To a solution of anhydrous dioxane (20 mL), N,N-Dimethylformamide (10 mL) and H₂O (5 mL), compound **4** (235 mg, 0.5 mmol, 1 equiv), compound **3** (1 g, 3 mmol, 6 equiv), K₂CO₃ (1.66 g, 12 mmol, 24 equiv) and Pd(dppf)Cl₂ (110 mg, 0.15 mmol, 0.3 equiv) were added and the mixture was stirred at 90 °C overnight under N₂ atmosphere to give a black solution. The crude product was purified by column chromatography (SiO₂, DCM/MeOH, v/v = 50/1) to afford ligand **L** as a white powder (150 mg, 30%). ¹H NMR (400 MHz, CDCl₃, 298 K): δ = 8.96 (s, 1H), 8.68–8.64 (m, 1H), 8.21 (s, 1H), 8.03–7.96 (t, 1H), 7.96–7.88 (m, 2H), 7.82 (m, 1H), 7.77 (s, 1H), 6.51–6.46 (t, 1H).

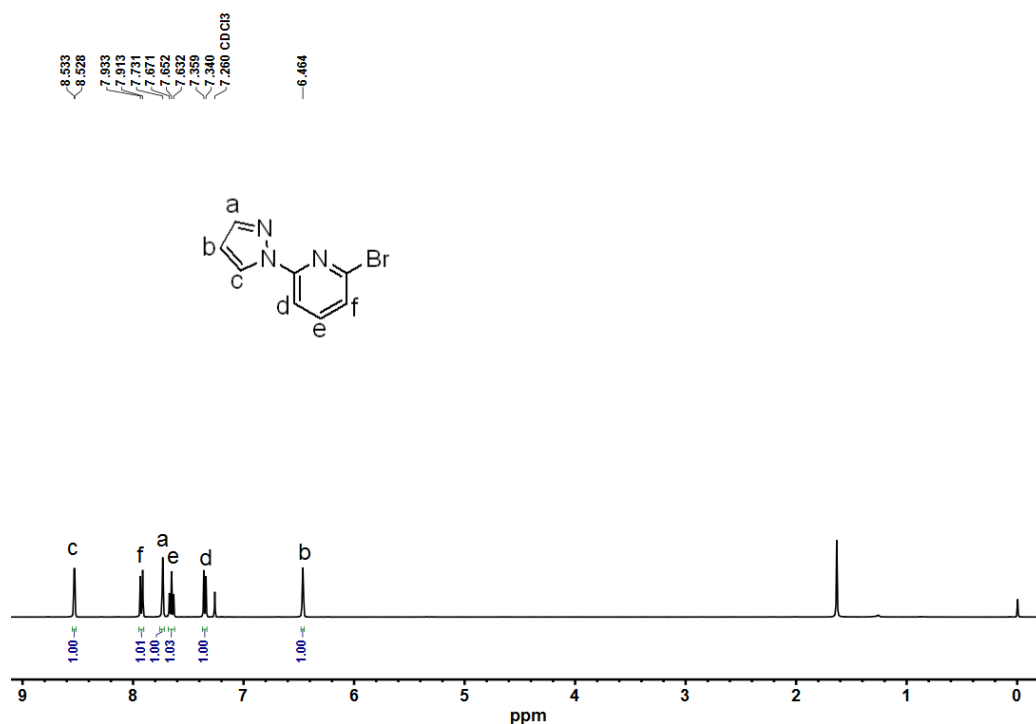


Figure S1. ¹H-NMR spectrum of **1** (400 MHz, CDCl₃, 298 K).

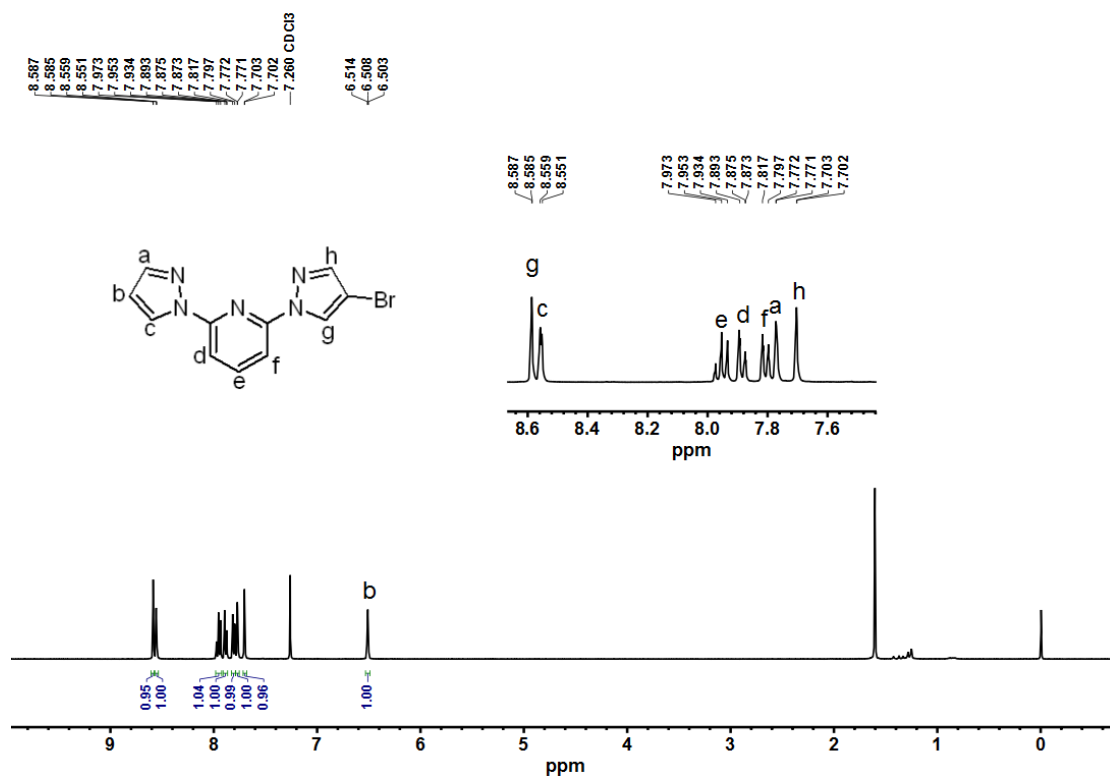


Figure S2. ¹H-NMR spectrum of **2** (400 MHz, CDCl₃, 298 K).

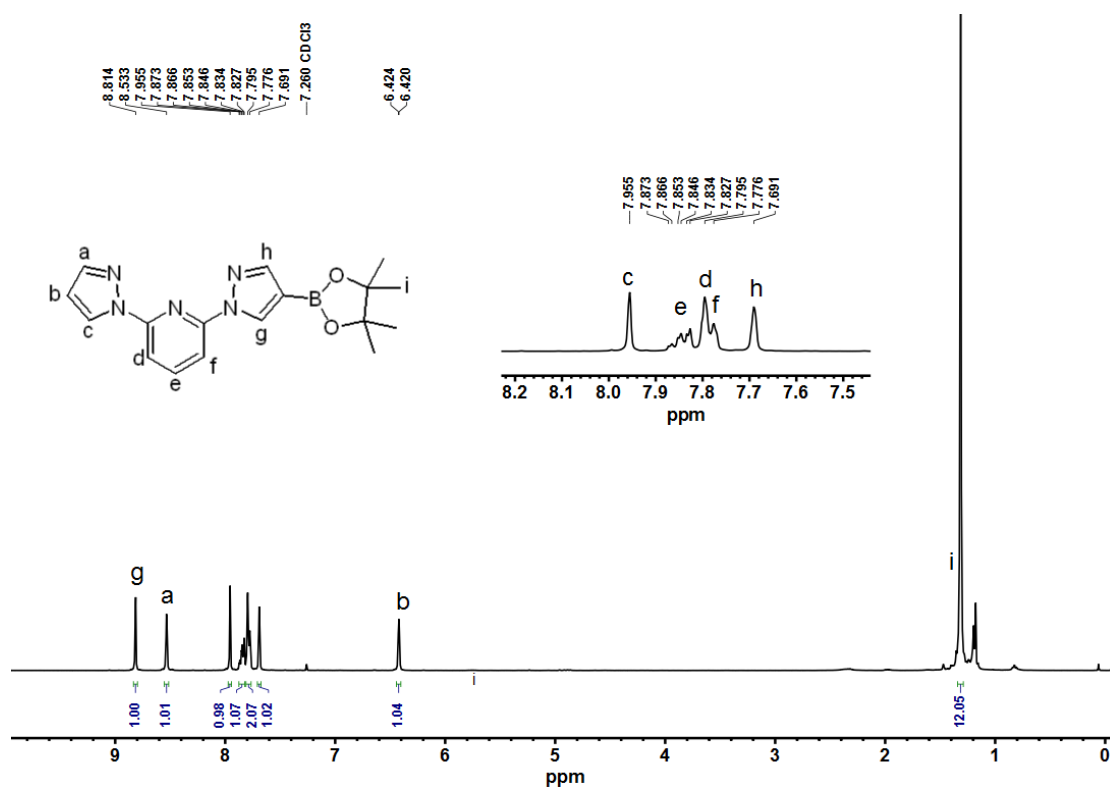


Figure S3. ¹H-NMR spectrum of **3** (400 MHz, CDCl₃, 298 K).

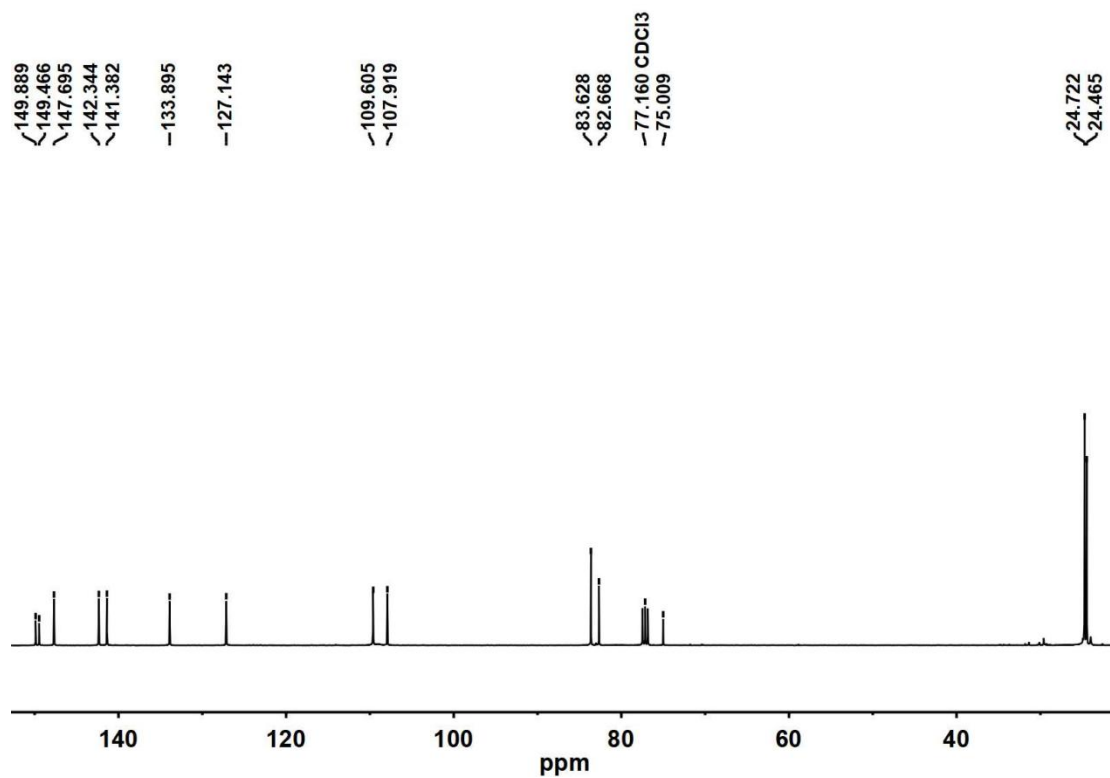


Figure S4. ^{13}C -NMR spectrum of **3** (101 MHz, CDCl_3 , 298 K).

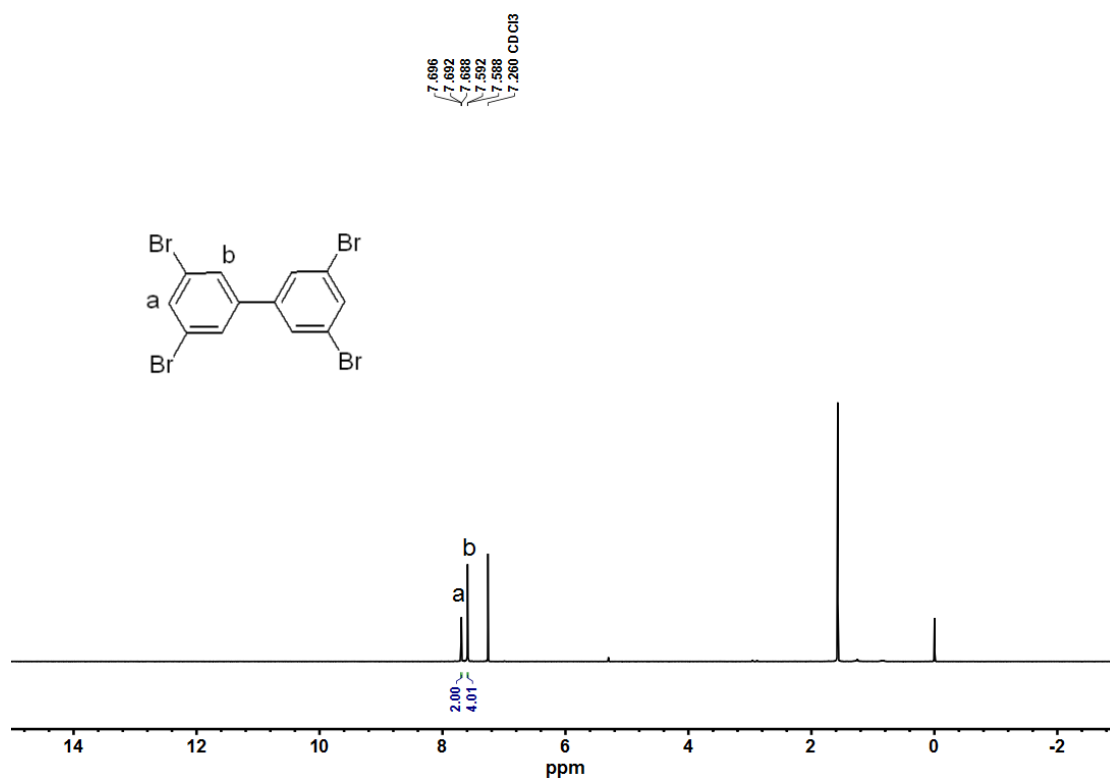


Figure S5. ^1H -NMR spectrum of **4** (400 MHz, CDCl_3 , 298 K).

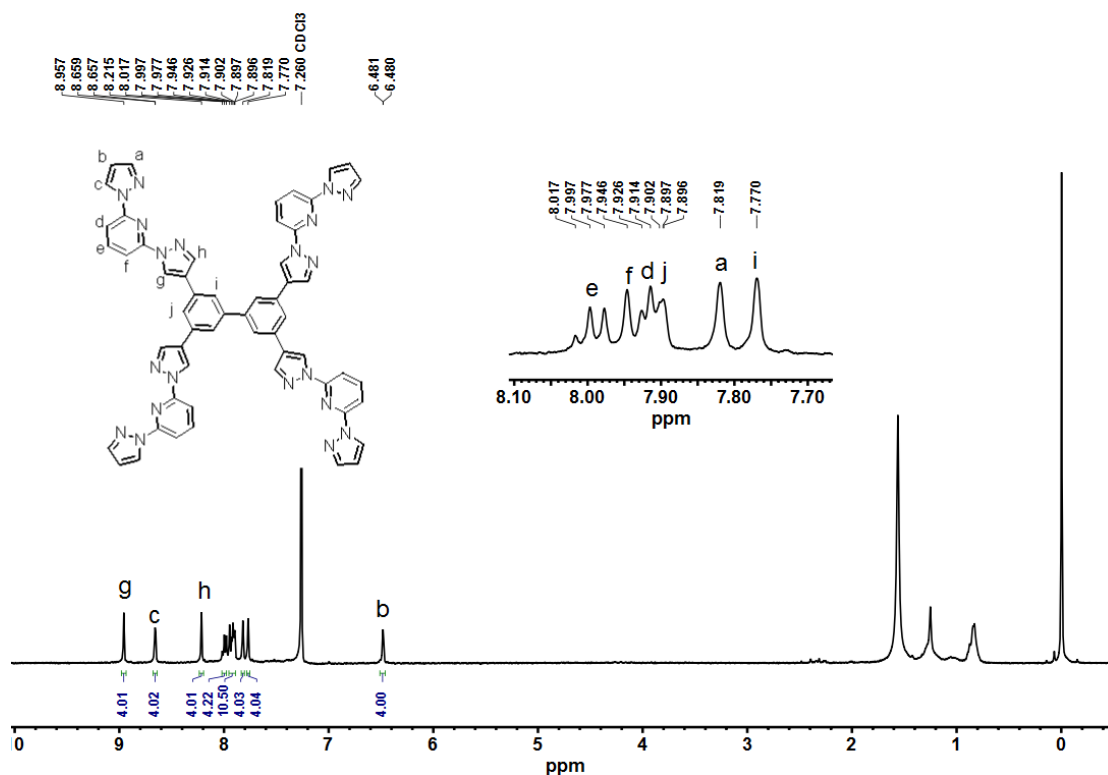


Figure S6. $^1\text{H-NMR}$ spectrum of **L** (400 MHz, CDCl_3 , 298 K).

2.2 Synthesis and characterization of cages.

Initially, the ligand **L** (3.0 equiv) was treated with Ln ions (4.0 equiv) in acetonitrile to fabricate the Ln_8L_6 type structure. However, the suspension of the reaction system can't turn clear. Interestingly, when another 2.0 quive lanthanide ions (metal-to-ligand ratio = 2:1) was added into above solution, the solution gradually turned into homogeneous clear soluton after stried for several minutes. This result indicates that the self-assembly occur in a 2:1 metal-to-ligand ratio, other than 4:3.

Synthesis and characterization of Ln_4L_2 :

The mixture of $\text{La}(\text{CF}_3\text{SO}_3)_3$ (11.72 mg, 20 mmol, 2 eq), **L** (10.07 mg, 10 mmol, 1 eq) and 1 mL CD_3CN were sealed in a galss bottle and then stirred at 70°C for 20 minutes. This solution was characterized without further treatment. The synthesis procedures of Nd_4L_2 is similar with that of La_4L_2 by changing the $\text{La}(\text{CF}_3\text{SO}_3)_3$ to $\text{Nd}(\text{CF}_3\text{SO}_3)_3$.

The $^1\text{H NMR}$ spectrum of La_4L_2 (400 MHz, CD_3CN , 298 K): $\delta = 9.22$ (s, 1H), 8.92 (s, 1H), 8.87 (d, $J = 2.7$ Hz, 1H), 8.72 (d, $J = 2.5$ Hz, 1H), 8.33 (t, $J = 8.1$ Hz, 1H), 8.19

(s, 1H), 8.05 (d, J = 8.2 Hz, 2H), 7.99 (t, J = 8.0 Hz, 2H), 7.94 (s, 1H), 7.88 (t, J = 8.1 Hz, 3H), 7.83 (s, 1H), 7.77 (d, J = 8.1 Hz, 1H), 7.61 (s, 1H), 7.49 (s, 2H), 6.92 – 6.89 (m, 2H), 6.83 (s, 1H). ESI-TOF-MS for La_4L_2 showed continuous losing of the OTf^- anions: m/z calcd for $[\text{La}_4\text{L}_2(\text{OTf})_{10}]^{2+}$ 2013.4328, found 2013.4301; calcd for $[\text{La}_4\text{L}_2(\text{OTf})_9]^{3+}$ 1292.6377, found 1292.6353; calcd for $[\text{La}_4\text{L}_2(\text{OTf})_8]^{4+}$ 932.2399, found 932.2380; calcd for $[\text{La}_4\text{L}_2(\text{OTf})_7]^{5+}$ 716.0061, found 715.9999.

ESI-TOF-MS of Nd_4L_2 : calcd for $[\text{Nd}_4\text{L}_2(\text{OTf})_{10}]^{2+}$ 2022.4394, found 2022.4315; calcd for $[\text{Nd}_4\text{L}_2(\text{OTf})_9]^{3+}$ 1298.6421, found 1298.6420; calcd for $[\text{Nd}_4\text{L}_2(\text{OTf})_8]^{4+}$ 936.7434, found 936.7424; calcd for $[\text{Nd}_4\text{L}_2(\text{OTf})_7]^{5+}$ 719.6042, found 719.6033.

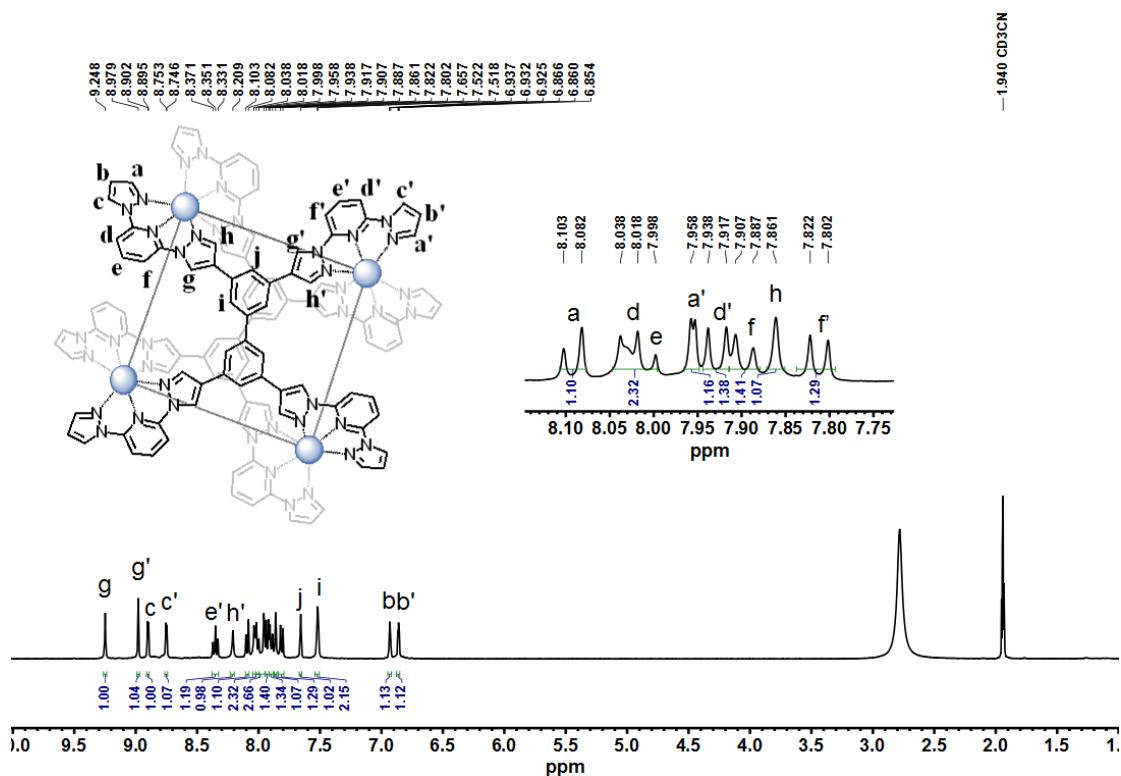


Figure S7. ^1H -NMR spectrum of La_4L_2 (400 MHz, CD_3CN , 298 K).

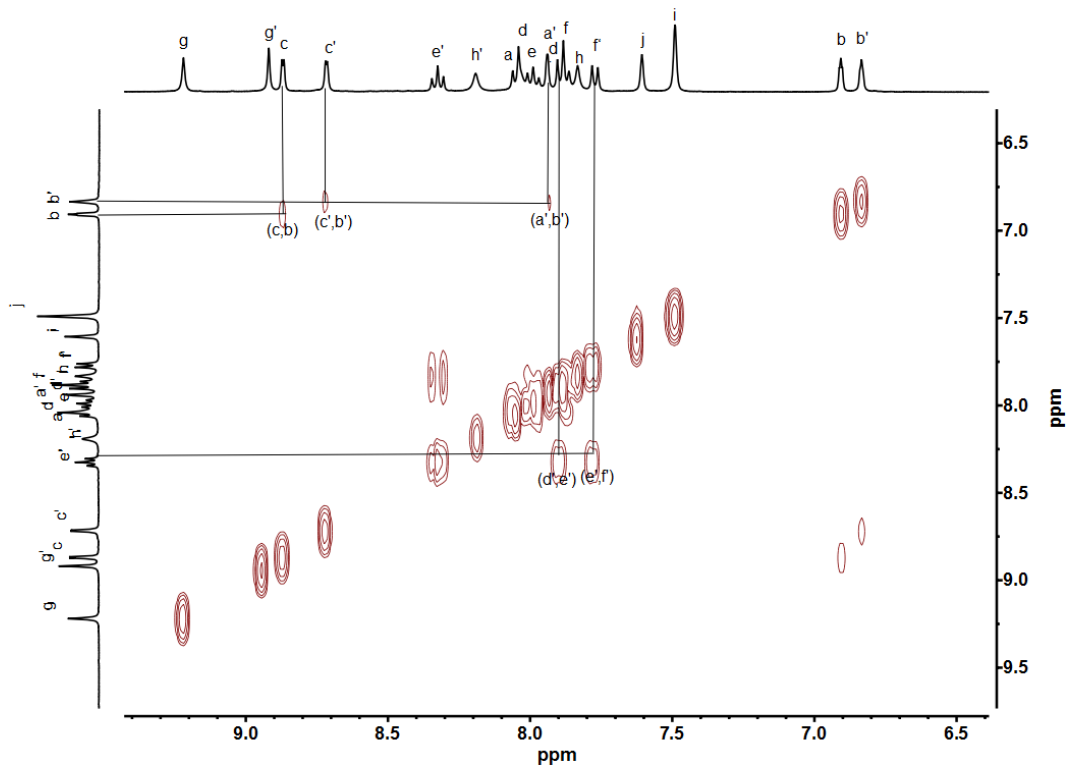


Figure S8. ^1H - ^1H COSY spectrum of La_4L_2 (400 MHz, CD_3CN , 298 K).

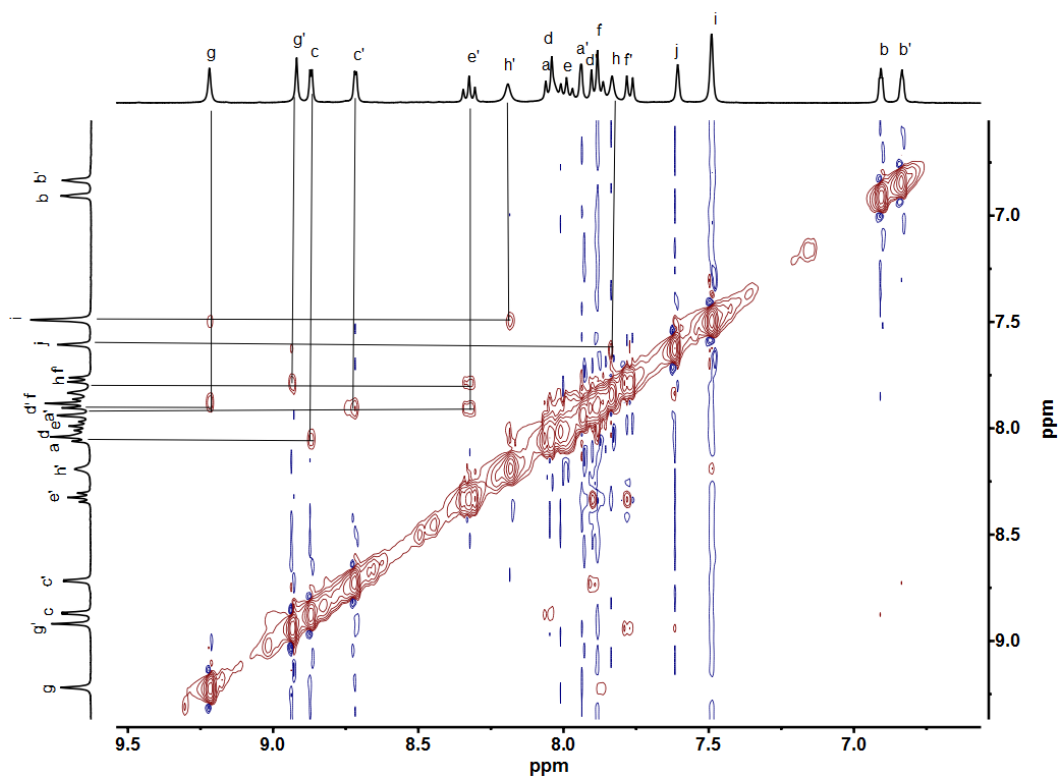


Figure S9. ^1H - ^1H NOESY spectrum of La_4L_2 (400 MHz, CD_3CN , 298 K).

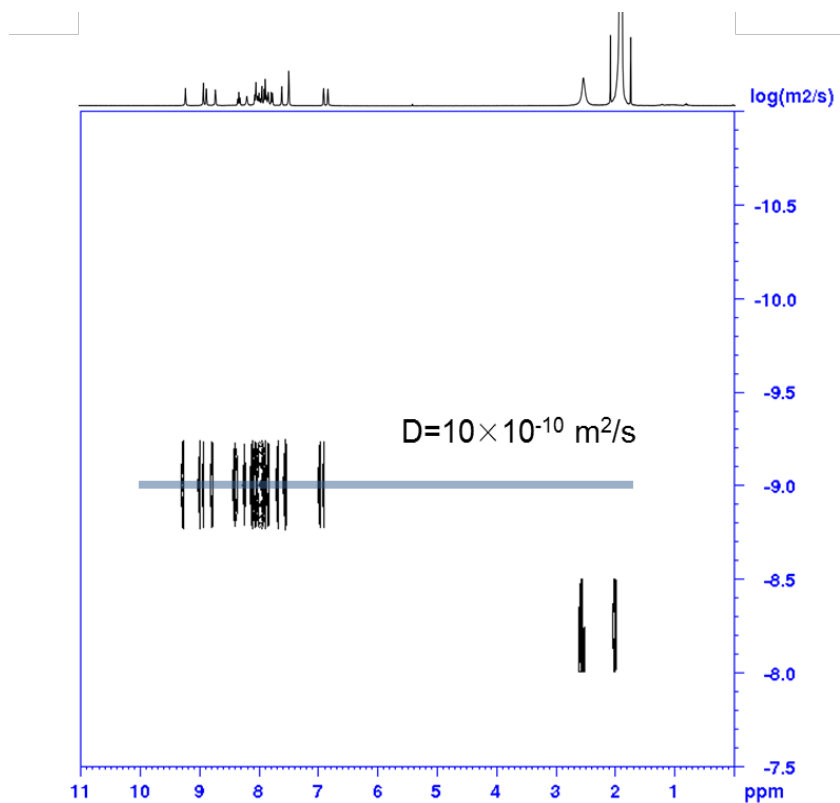


Figure S10. ^1H - ^1H DOSY spectrum of La_4L_2 (400 MHz, CD_3CN , 298 K).

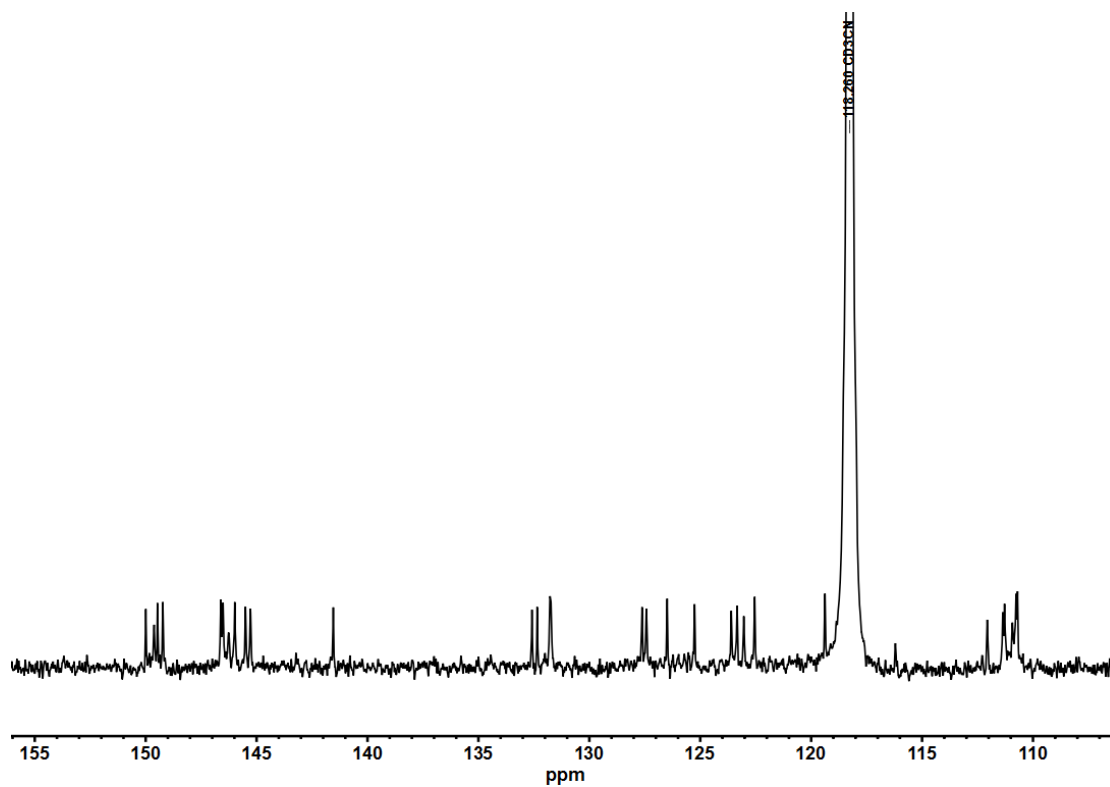


Figure S11. ^{13}C -NMR spectrum of La_4L_2 (101 MHz, CD_3CN , 298 K).

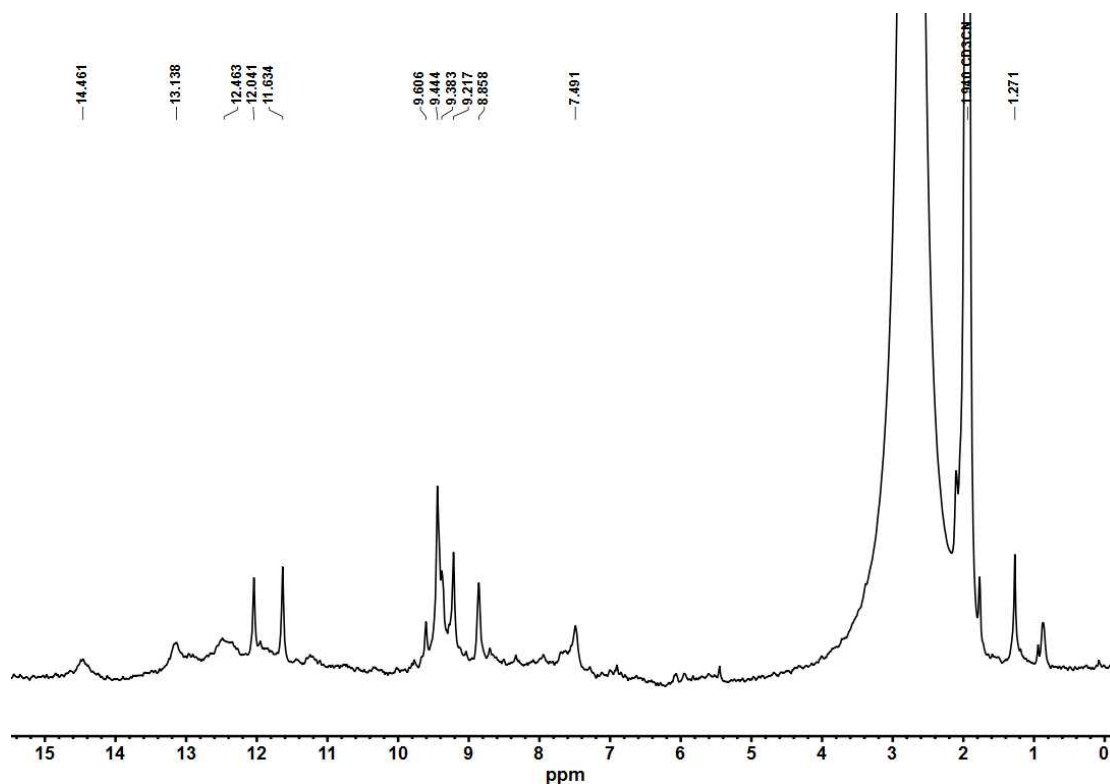


Figure S12. ^1H -NMR spectrum of Nd_4L_2 (400 MHz, CD_3CN , 298 K).

Synthesis and characterization of Ln_8L_4 :

The mixture of $\text{Sm}(\text{CF}_3\text{SO}_3)_3$ (11.95 mg, 20 mmol, 2 eq), **L** (10.07 mg, 10 mmol, 1 eq) and 1 mL CD_3CN were sealed in a glass bottle and then stirred at 70 °C for 20 minutes. This solution was characterized without further treatment. ^1H NMR spectra showed the quantitative formation of Sm_8L_4 . By changing the $\text{Sm}(\text{CF}_3\text{SO}_3)_3$ to $\text{Eu}(\text{CF}_3\text{SO}_3)_3$, $\text{Tb}(\text{CF}_3\text{SO}_3)_3$, $\text{Dy}(\text{CF}_3\text{SO}_3)_3$ and $\text{Ho}(\text{CF}_3\text{SO}_3)_3$, Ln_8L_4 structure similar to Sm_8L_4 can be obtained.

The ^1H NMR spectrum of Sm_8L_4 (400 MHz, CD_3CN , 298 K): δ = 9.66 (s, 1H), 9.35 (s, 1H), 9.14 (d, J = 13.5 Hz, 2H), 8.96 (d, J = 3.0 Hz, 1H), 8.84 (s, 1H), 8.79 (d, J = 2.8 Hz, 1H), 8.72–8.67 (m, 2H), 8.62 (dd, J = 5.5, 2.9 Hz, 2H), 8.57 (t, J = 8.4 Hz, 1H), 8.53 (s, 0H), 8.45 (t, J = 8.2 Hz, 1H), 8.38 (d, J = 8.4 Hz, 1H), 8.27 (d, J = 8.3 Hz, 1H), 8.15–8.06 (m, 2H), 8.00 (dd, J = 14.0, 8.3 Hz, 2H), 7.95–7.90 (m, 1H), 7.88–7.83 (m, 2H), 7.81 (s, 2H), 7.66 (s, 1H), 7.60 (s, 1H), 7.46 (d, J = 8.4 Hz, 3H), 7.23 (d, J = 9.2 Hz, 2H), 7.00 (s, 1H), 6.91 (d, J = 2.5 Hz, 1H), 6.86 (d, J = 2.6 Hz, 1H), 6.68 (t, J = 2.3 Hz, 1H), 6.55 (t, J = 2.3 Hz, 1H), 5.98 (s, 1H). ESI-TOF-MS for Sm_8L_4 showed

continuous losing of the OTf⁻ anions: m/z calcd for [Sm₈L₄(OTf)₂₀]⁴⁺ 2027.4540, found 2027.4610; calcd for [Sm₈L₄(OTf)₁₉]⁵⁺ 1600.1756, found 1600.1769; calcd for [Sm₈L₄(OTf)₁₈]⁶⁺ 1308.6543, found 1308.6549; calcd for [Sm₈L₄(OTf)₁₇]⁷⁺ 1100.4247, found 1100.4248; calcd for [Sm₈L₄(OTf)₁₆]⁸⁺ 944.3526, found 944.3536; calcd for [Sm₈L₄(OTf)₁₅]⁹⁺ 822.7853, found 822.7847.

The ¹H NMR spectrum of Eu₈L₄ (400 MHz, CD₃CN, 298 K): δ = 8.49 (s, 1H), 8.21 (s, 1H), 8.13 (s, 1H), 7.92 (s, 2H), 7.83 (s, 1H), 7.66 (s, 1H), 7.54 (s, 1H), 7.35 (s, 1H), 6.81 (s, 1H), 6.64 (s, 1H), 6.10 (s, 1H), 5.92 (d, J = 20.7 Hz, 3H), 5.78 (d, J = 7.8 Hz, 2H), 5.73–5.62 (m, 3H), 5.38 (s, 2H), 5.22–5.09 (m, 3H), 4.88 (s, 3H), 4.65 (s, 1H), 4.51 (s, 1H), 4.41 (s, 1H), 4.27 (s, 2H), 4.15 (s, 1H), 4.05 (s, 1H), 3.22 (s, 2H). ESI-TOF-MS of Eu₈L₄: calcd for [Eu₈L₄(OTf)₁₉]⁵⁺ 1602.3782, found 1602.3752; calcd for [Eu₈L₄(OTf)₁₈]⁶⁺ 1310.4897, found 1310.4875; calcd for [Eu₈L₄(OTf)₁₇]⁷⁺ 1101.8580, found 1101.8536; calcd for [Eu₈L₄(OTf)₁₆]⁸⁺ 945.6054, found 945.5032; calcd for [Eu₈L₄(OTf)₁₅]⁹⁺ 824.0090, found 824.0077.

ESI-TOF-MS of Tb₈L₄: calcd for [Tb₈L₄(OTf)₂₁]³⁺ 2788.2771, found 2788.2810; calcd for [Tb₈L₄(OTf)₂₀]⁴⁺ 2053.9697, found 2053.9702; calcd for [Tb₈L₄(OTf)₁₉]⁵⁺ 1613.1868, found 1613.1853; calcd for [Tb₈L₄(OTf)₁₈]⁶⁺ 1319.4955, found 1319.4955; calcd for [Tb₈L₄(OTf)₁₇]⁷⁺ 1110.0035, found 1110.0028; calcd for [Tb₈L₄(OTf)₁₆]⁸⁺ 925.6340, found 925.6337; calcd for [Tb₈L₄(OTf)₁₅]⁹⁺ 833.3481, found 833.3492.

ESI-TOF-MS of Dy₈L₄: calcd for [Dy₈L₄(OTf)₂₀]⁴⁺ 2060.4759, found 2060.4780; calcd for [Dy₈L₄(OTf)₁₉]⁵⁺ 1619.1906, found 1619.8886; calcd for [Dy₈L₄(OTf)₁₈]⁶⁺ 1324.5001, found 1324.4993; calcd for [Dy₈L₄(OTf)₁₇]⁷⁺ 1114.0069, found 1114.0051; calcd for [Dy₈L₄(OTf)₁₆]⁸⁺ 956.1369, found 956.1371; calcd for [Dy₈L₄(OTf)₁₅]⁹⁺ 833.3492, found 833.3481.

ESI-TOF-MS of Ho₈L₄: calcd for [Ho₈L₄(OTf)₂₀]⁴⁺ 2065.4807, found 2065.4768; calcd for [Ho₈L₄(OTf)₁₉]⁵⁺ 1622.5941, found 1622.5909; calcd for [Ho₈L₄(OTf)₁₈]⁶⁺ 1327.3368, found 1327.3330; calcd for [Ho₈L₄(OTf)₁₇]⁷⁺ 1167.4379, found 1167.4352; calcd for [Ho₈L₄(OTf)₁₆]⁸⁺ 985.2641, found 985.2610; calcd for [Ho₈L₄(OTf)₁₅]⁹⁺ 835.2400, found 835.2360.

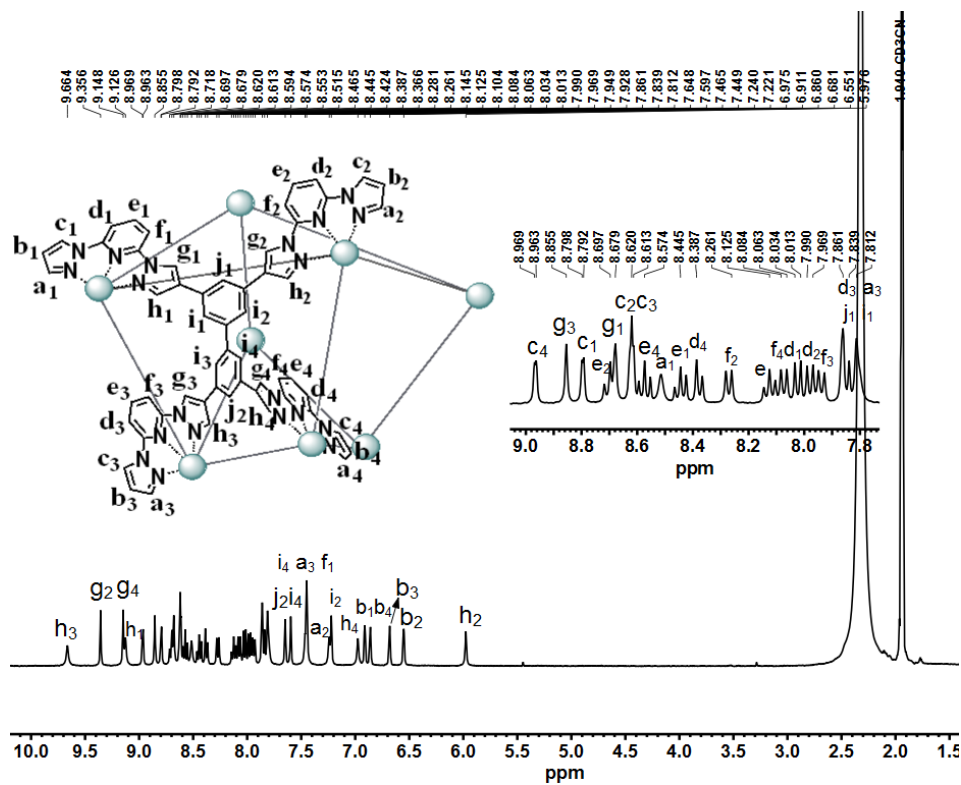


Figure S13. ^1H -NMR spectrum of Sm_8L_4 (400 MHz, CD_3CN , 298 K).

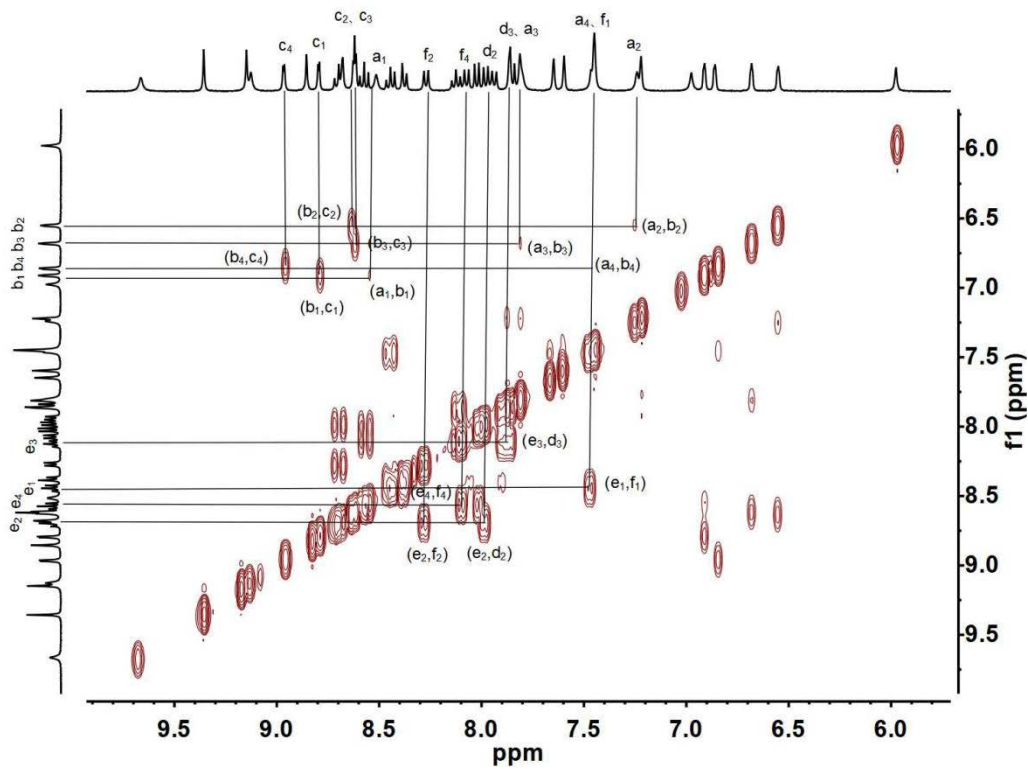


Figure S14. ^1H - ^1H COSY spectrum of Sm_8L_4 (400 MHz, CD_3CN , 298 K).

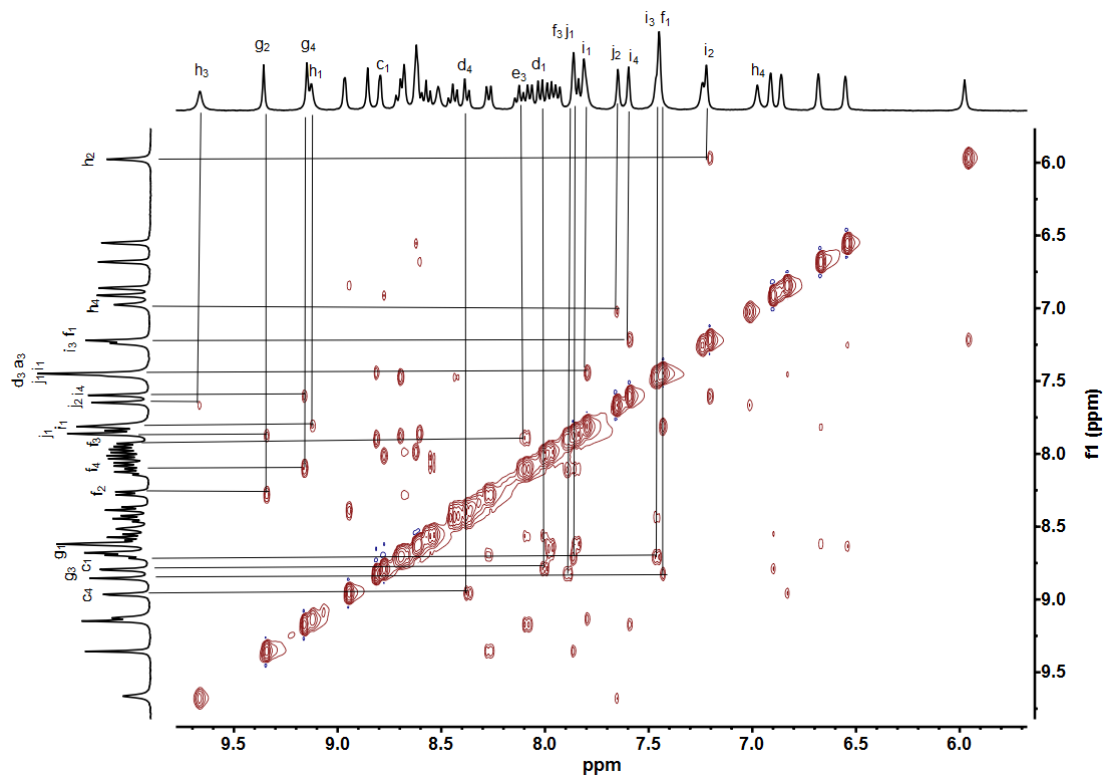


Figure S15. ¹H-¹H NOESY spectrum of Sm₈L₄ (400 MHz, CD₃CN, 298 K).

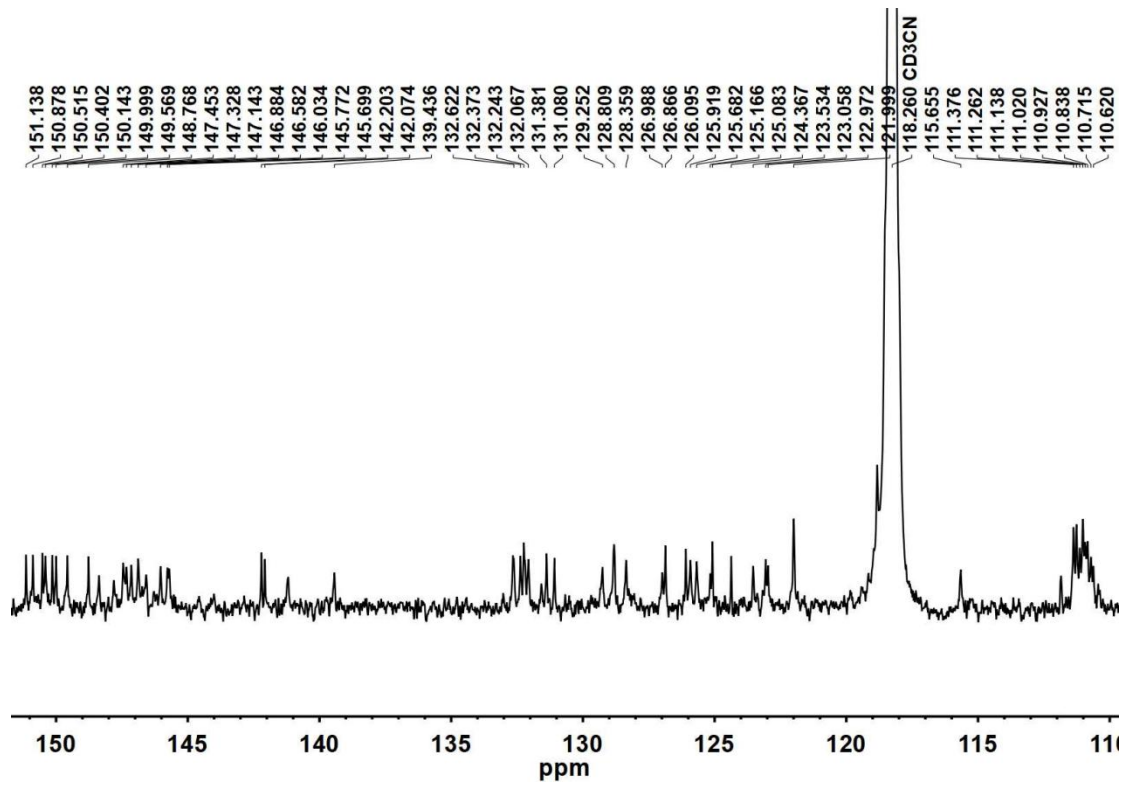


Figure S16. ¹³C-NMR spectrum of Sm₈L₄ (101 MHz, CD₃CN, 298 K).

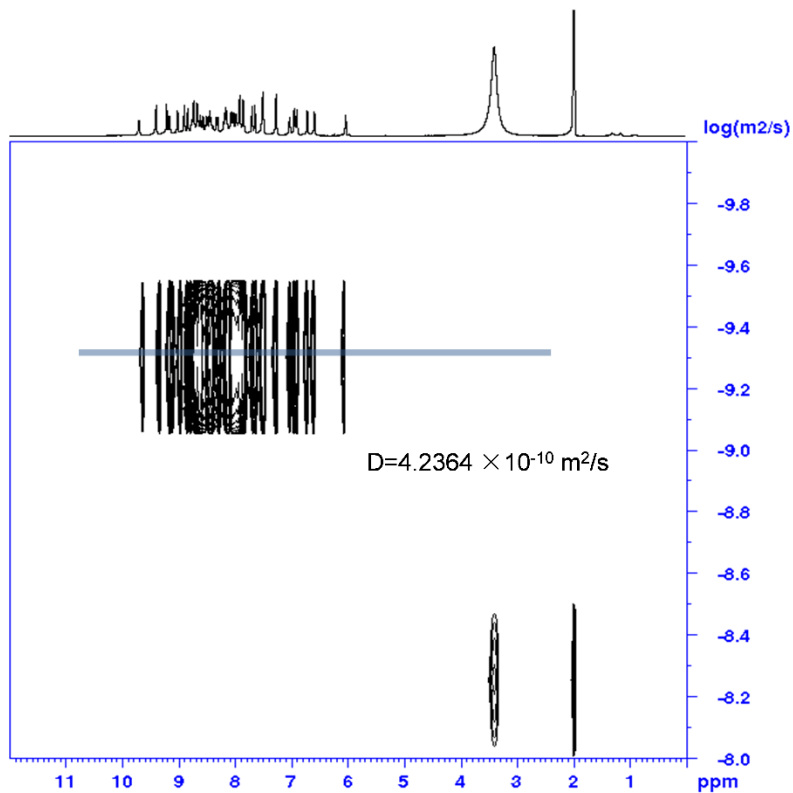


Figure S17. ^1H - ^1H DOSY spectrum of Sm_8L_4 (400 MHz, CD_3CN , 298 K).

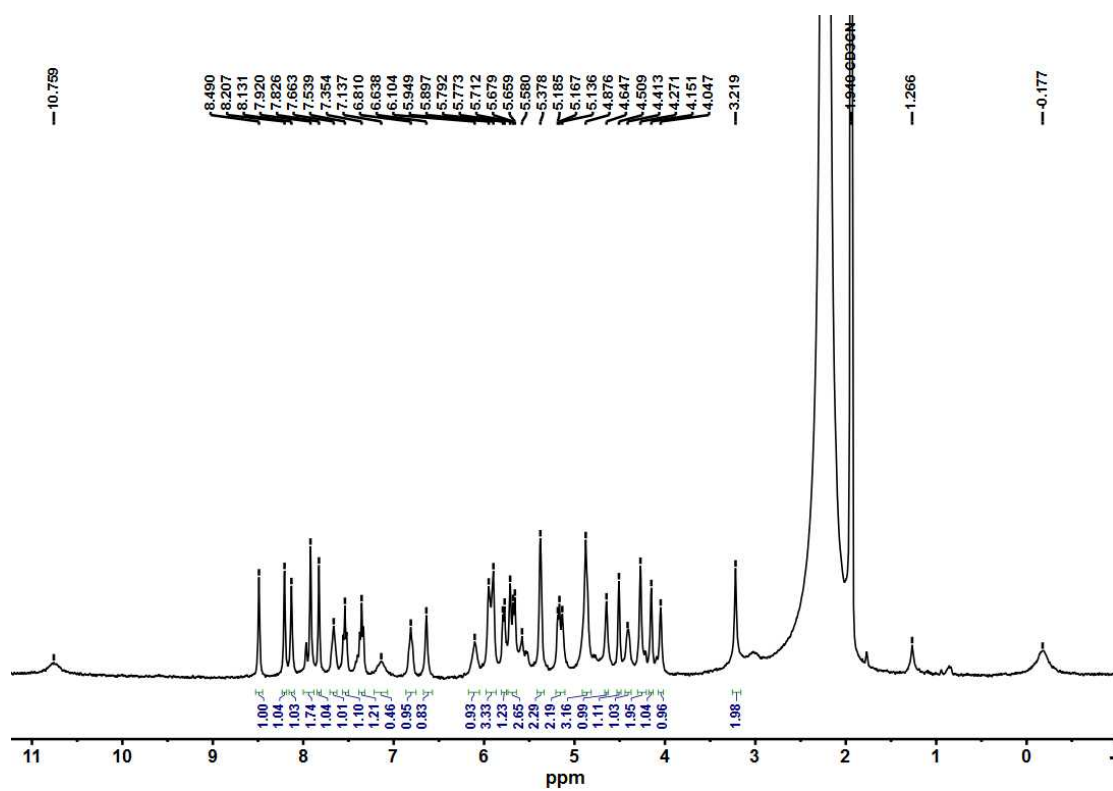


Figure S18. ^1H -NMR spectrum of Eu_8L_4 (400 MHz, CD_3CN , 298 K).

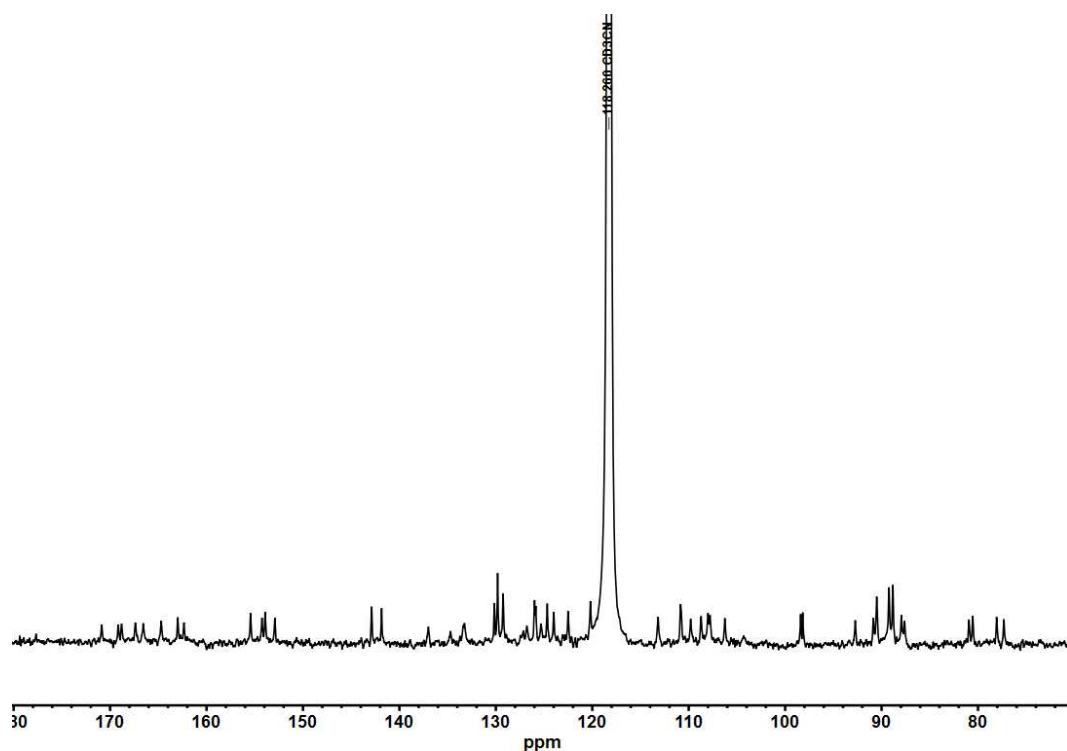


Figure S19. ^{13}C -NMR spectrum of Eu_8L_4 (101 MHz, CD_3CN , 298 K).

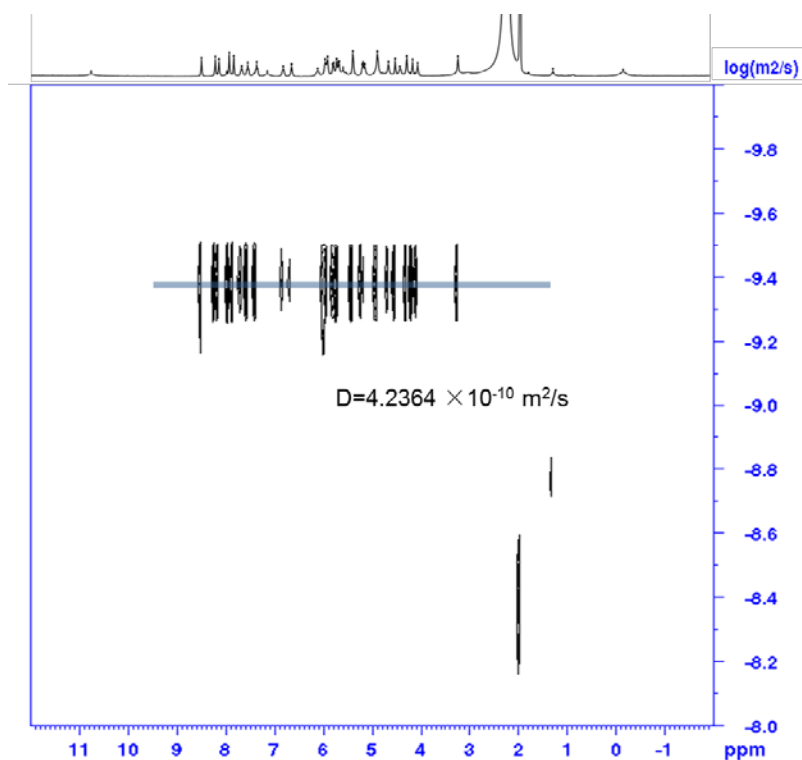


Figure S20. ^1H - ^1H DOSY spectrum of Eu_8L_4 (400 MHz, CD_3CN , 298 K).

Synthesis and characterization of mixed Ln_8L_4 and Ln_6L_3 :

The mixture of $\text{Lu}(\text{CF}_3\text{SO}_3)_3$ (12.44 mg, 20 mmol, 2 eq), **L** (10.07 mg, 10 mmol, 1 eq) and 1 mL CD_3CN were sealed in a glass bottle and then stirred at 70 °C for 20 minutes.

This solution was characterized without further treatment. ^1H NMR spectra and ESI - MS spectra showed the formation of Lu_8L_4 and Lu_6L_3 mixture. Similar mixture were also observed in the assembly solution of ligand **L** and $\text{Er}(\text{CF}_3\text{SO}_3)_3$.

ESI-TOF-MS of Er_8L_4 : calcd for $[\text{Er}_8\text{L}_4(\text{OTf})_{20}]^{4+}$ 2069.9739, found 2069.9736; calcd for $[\text{Er}_8\text{L}_4(\text{OTf})_{19}]^{5+}$ 1626.1966, found 1626.1952; calcd for $[\text{Er}_8\text{L}_4(\text{OTf})_{18}]^{6+}$ 1130.3384, found 1130.3337; calcd for $[\text{Er}_8\text{L}_4(\text{OTf})_{17}]^{7+}$ 1119.0111, found 1119.0070; calcd for $[\text{Er}_8\text{L}_4(\text{OTf})_{16}]^{8+}$ 960.6411, found 960.6378; calcd for $[\text{Er}_8\text{L}_4(\text{OTf})_{15}]^{9+}$ 835.2400, found 835.2360. calcd for $[\text{Er}_6\text{L}_3(\text{OTf})_{14}]^{4+}$ 1515.4988, found 1515.4997; calcd for $[\text{Er}_6\text{L}_3(\text{OTf})_{13}]^{5+}$ 1182.6092, found 1182.6077; calcd for $[\text{Er}_8\text{L}_4(\text{OTf})_{12}]^{6+}$ 960.6823, found 960.6805.

ESI-TOF-MS of Lu_8L_4 : calcd for $[\text{Lu}_8\text{L}_4(\text{OTf})_{19}]^{5+}$ 1638.6108, found 1638.6150; calcd for $[\text{Lu}_8\text{L}_4(\text{OTf})_{18}]^{6+}$ 1340.6836, found 1340.6809; calcd for $[\text{Lu}_8\text{L}_4(\text{OTf})_{17}]^{7+}$ 1127.8784, found 1127.8806; calcd for $[\text{Lu}_8\text{L}_4(\text{OTf})_{16}]^{8+}$ 968.2745, found 968.2791. calcd for $[\text{Lu}_6\text{L}_3(\text{OTf})_{14}]^{4+}$ 1526.7627, found 1526.7579; calcd for $[\text{Lu}_6\text{L}_3(\text{OTf})_{13}]^{5+}$ 1191.6172, found 1191.6196; calcd for $[\text{Lu}_6\text{L}_3(\text{OTf})_{12}]^{6+}$ 968.1882, found 968.1909; calcd for $[\text{Lu}_6\text{L}_3(\text{OTf})_{11}]^{7+}$ 808.5953, found 808.5990.

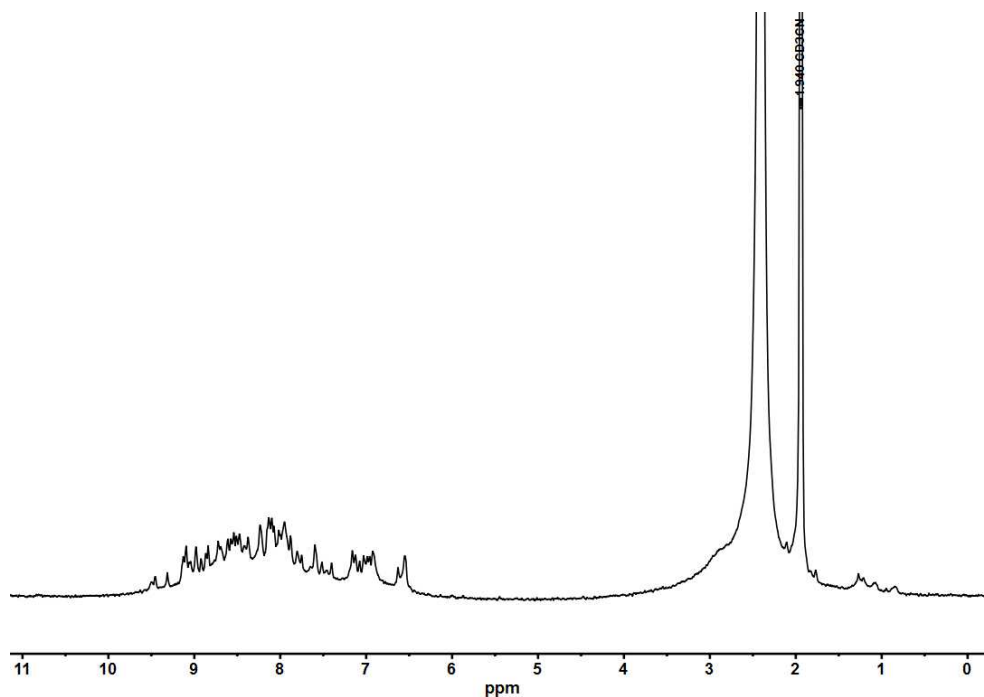


Figure S21. ^1H -NMR spectrum of the assembly that fabricated by ligand **L** and $\text{Lu}(\text{CF}_3\text{SO}_3)_3$ in a ratio of 1:2 (400 MHz, CD_3CN , 298 K).

Structural and characterization of the assembly with excess lanthanide ions

The mixture of $\text{Sm}(\text{CF}_3\text{SO}_3)_3$ (23.8 mg, 40 μmol , 4 eq), **L** (10.07 mg, 10 μmol , 1 eq) and 1 mL CD_3CN were sealed in a glass bottle and then stirred at 70 °C for 10 minutes, or add 1 eq $\text{Sm}(\text{CF}_3\text{SO}_3)_3$ to the assembly solution of 1 eq Sm_8L_4 . This solution was characterized without further treatment. ESI-TOF-MS spectra showed the formation of Sm_6L_3 . The synthesis procedures of Ln_6L_3 ($\text{Ln} = \text{Eu}^{3+}$ and Lu^{3+}) are similar with that of Sm_6L_3 by changing the $\text{Sm}(\text{CF}_3\text{SO}_3)_3$ to $\text{Eu}(\text{CF}_3\text{SO}_3)_3$ and $\text{Lu}(\text{CF}_3\text{SO}_3)_3$.

The ^1H NMR spectrum of Sm_6L_3 (400 MHz, CD_3CN , 298 K): $\delta = 9.34$ (s, 1H), 8.98 (s, 1H), 8.70 (s, 1H), 8.38 (t, $J = 8.1$ Hz, 1H), 8.29 (t, $J = 10.4$ Hz, 2H), 8.03 (d, $J = 8.1$ Hz, 1H), 7.87 (d, $J = 8.1$ Hz, 1H), 6.86 (s, 1H). ESI-TOF-MS of Sm_6L_3 : calcd for $[\text{Sm}_6\text{L}_3(\text{OTf})_{15}]^{3+}$ 2036.9560, found 2036.9584; calcd for $[\text{Sm}_6\text{L}_3(\text{OTf})_{14}]^{4+}$ 1490.7292, found 1490.7315; calcd for $[\text{Sm}_6\text{L}_3(\text{OTf})_{13}]^{5+}$ 1162.3925, found 1162.3954; calcd for $[\text{Sm}_6\text{L}_3(\text{OTf})_{12}]^{6+}$ 944.0018, found 944.0047; calcd for $[\text{Sm}_6\text{L}_3(\text{OTf})_{11}]^{7+}$ 787.7243, found 787.7254.

The ^1H NMR spectrum of Eu_6L_3 (400 MHz, CD_3CN , 298 K): $\delta = 8.14$ (s, 1H), 7.58 (s, 1H), 5.86 (d, $J = 18.1$ Hz, 2H), 5.46–5.07 (m, 3H), 4.53 (s, 2H). ESI-TOF-MS of Eu_6L_3 : calcd for $[\text{Eu}_6\text{L}_3(\text{OTf})_{15}]^{3+}$ 2040.2942, found 2040.2917; calcd for $[\text{Eu}_6\text{L}_3(\text{OTf})_{14}]^{4+}$ 1492.9825, found 1492.9832; calcd for $[\text{Eu}_6\text{L}_3(\text{OTf})_{13}]^{5+}$ 1164.5955, found 1164.5967; calcd for $[\text{Eu}_6\text{L}_3(\text{OTf})_{12}]^{6+}$ 945.6709, found 945.6721; calcd for $[\text{Eu}_6\text{L}_3(\text{OTf})_{11}]^{7+}$ 789.1532, found 789.1550.

The ^1H NMR spectrum of Lu_6L_3 (400 MHz, CD_3CN , 298 K): $\delta = 9.48$ (s, 1H), 8.96 (s, 1H), 8.71 (s, 1H), 8.53–8.46 (t, 1H), 8.34 (d, $J = 15.0$ Hz, 1H), 8.28 (s, 1H), 8.17 (d, $J = 8.3$ Hz, 1H), 7.94 (d, $J = 8.2$ Hz, 1H), 6.90 (s, 1H). ESI-TOF-MS of Lu_6L_3 : calcd for $[\text{Lu}_6\text{L}_3(\text{OTf})_{15}]^{3+}$ 2086.0013, found 2086.0054; calcd for $[\text{Lu}_6\text{L}_3(\text{OTf})_{14}]^{4+}$ 1527.2629, found 1527.2653; calcd for $[\text{Lu}_6\text{L}_3(\text{OTf})_{13}]^{5+}$ 1192.0198, found 1192.0214; calcd for $[\text{Lu}_6\text{L}_3(\text{OTf})_{12}]^{6+}$ 968.5244, found 968.5271; calcd for $[\text{Lu}_6\text{L}_3(\text{OTf})_{11}]^{7+}$ 808.8849, found 808.8862.

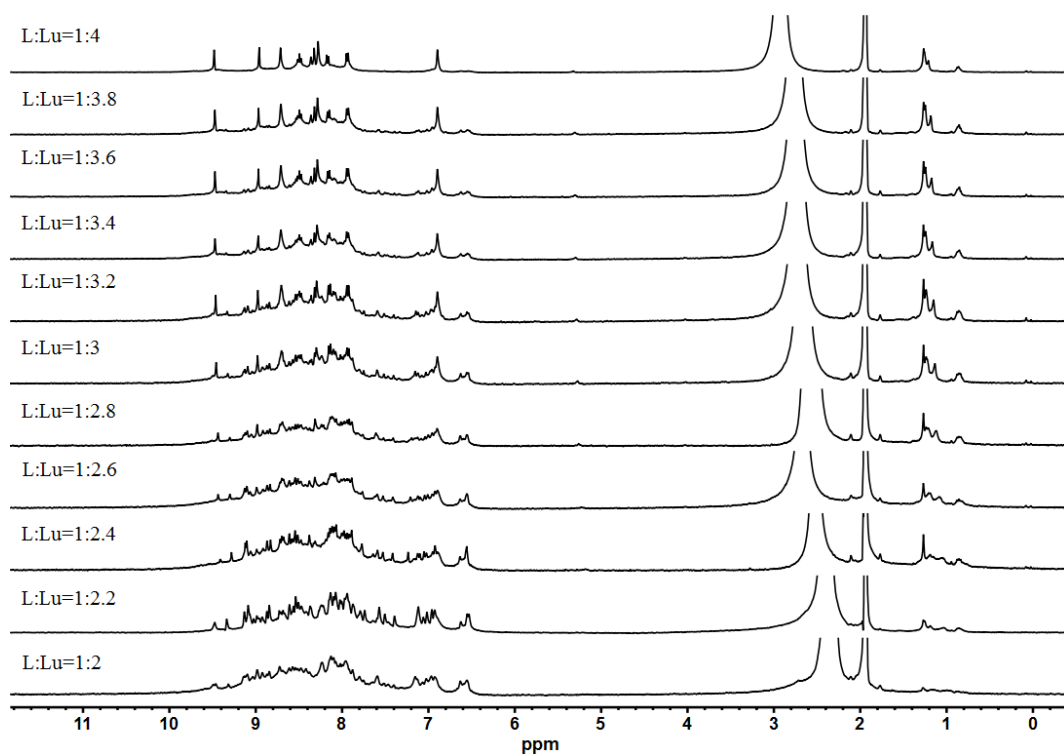


Figure S22. $^1\text{H-NMR}$ titration spectrum of ligand **L** and $\text{Lu}(\text{CF}_3\text{SO}_3)_3$ at different ratios (400 MHz, CD_3CN , 298 K).

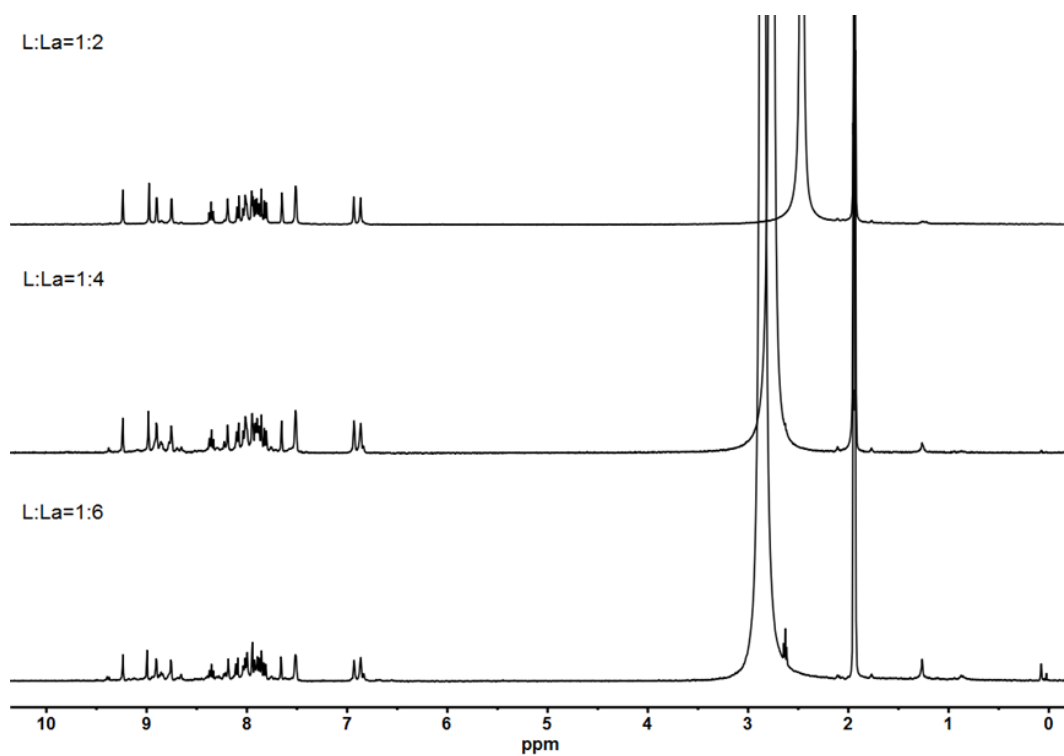


Figure S23. $^1\text{H-NMR}$ spectrum of ligand **L** and $\text{La}(\text{CF}_3\text{SO}_3)_3$ assembled in different ratios (400 MHz, CD_3CN , 298 K).

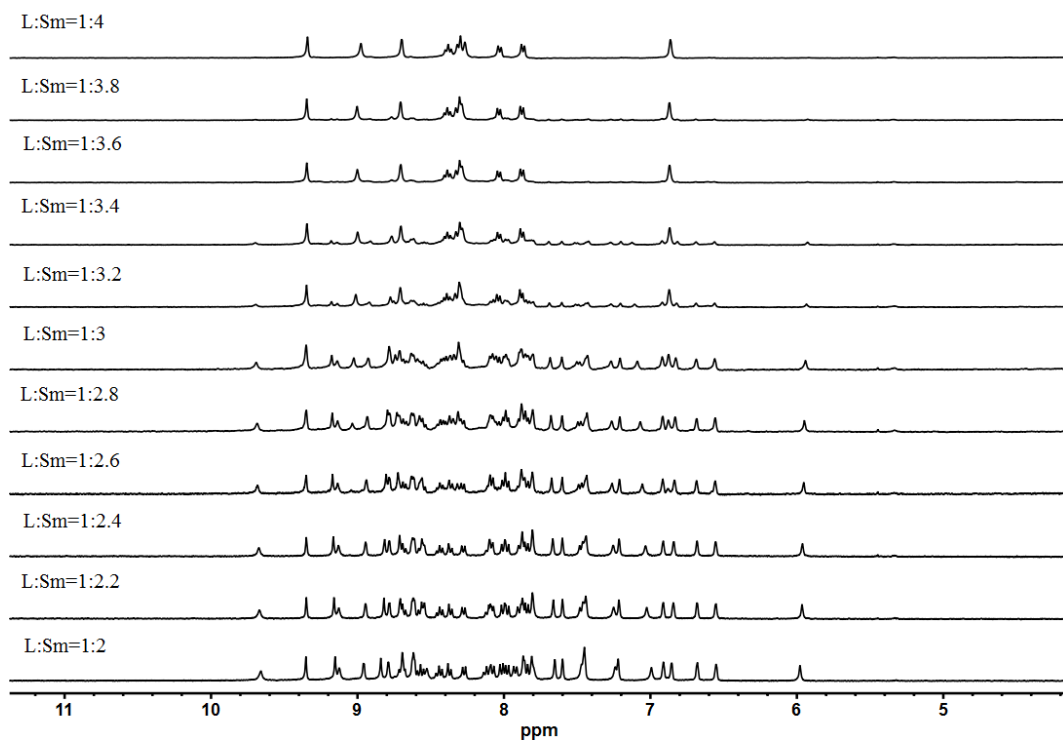


Figure S24. $^1\text{H-NMR}$ titration spectrum of ligand **L** and $\text{Sm}(\text{CF}_3\text{SO}_3)_3$ at different ratios (400 MHz, CD_3CN , 298 K).

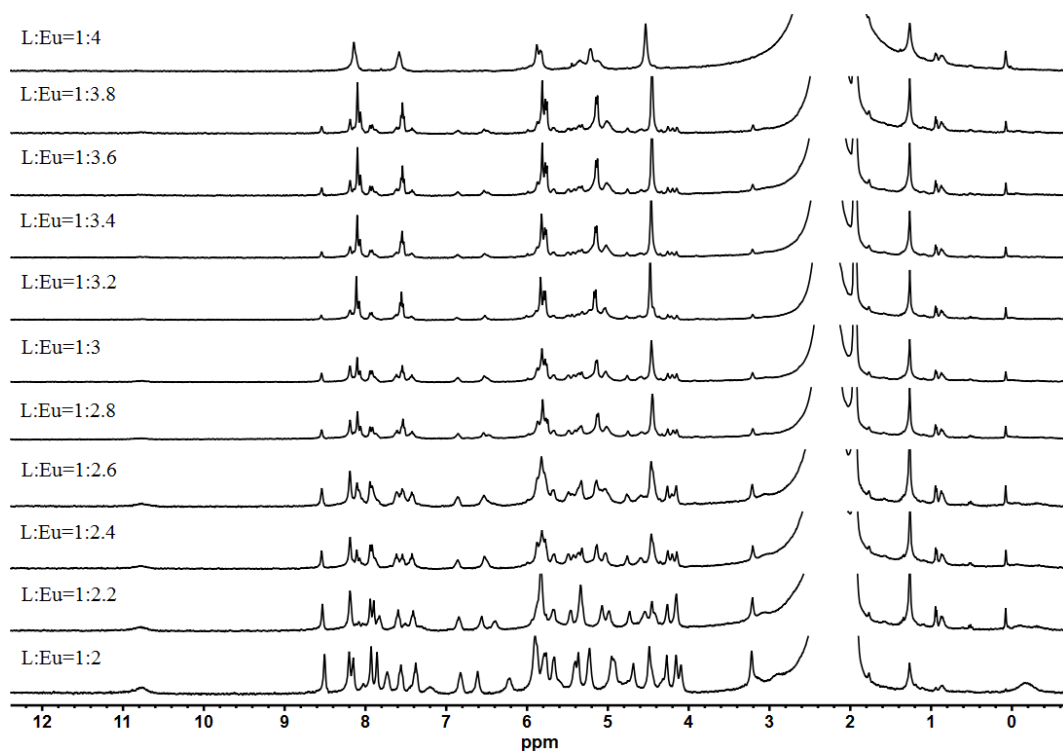


Figure S25. $^1\text{H-NMR}$ titration spectrum of ligand **L** and $\text{Eu}(\text{CF}_3\text{SO}_3)_3$ at different ratios (400 MHz, CD_3CN , 298 K).

2.3 ESI-TOF-MS spectra

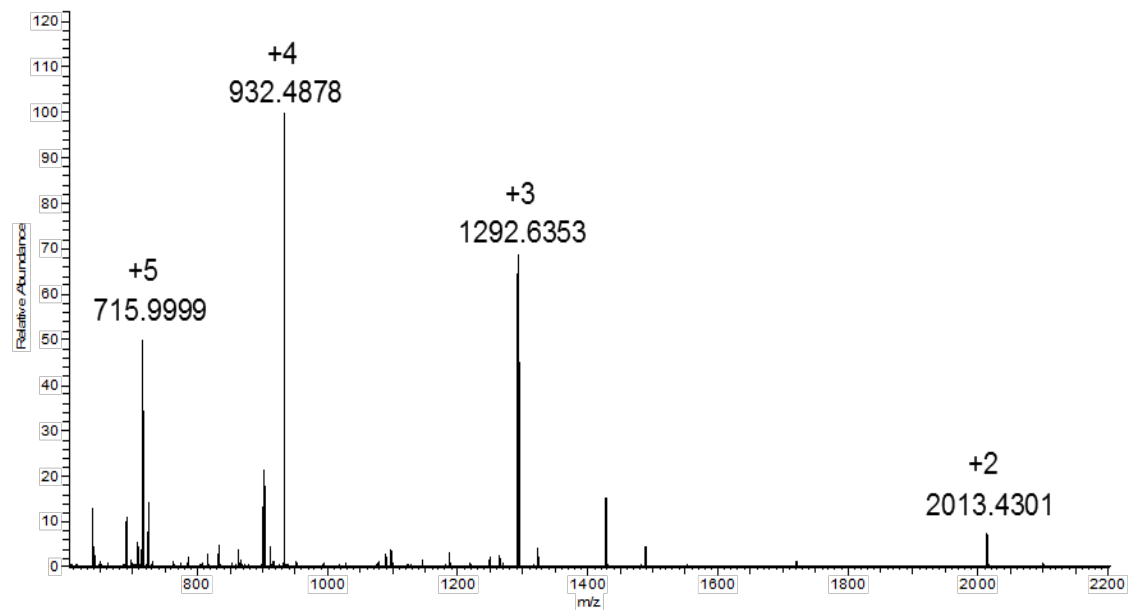


Figure S26. ESI-TOF-MS of complex La_4L_2 .

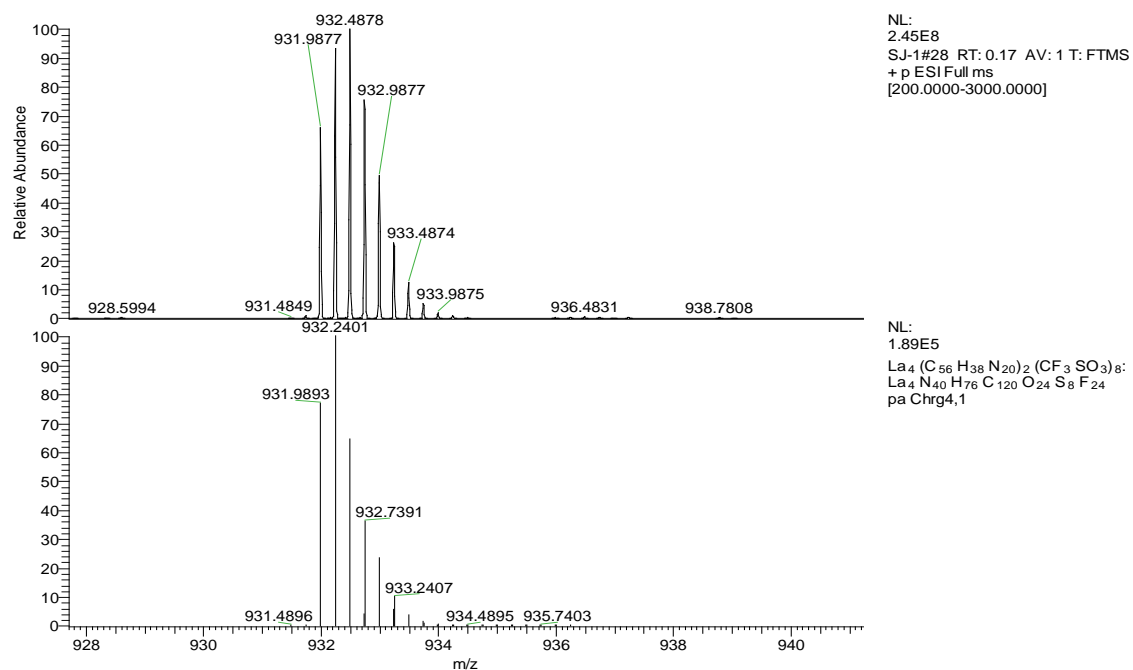


Figure S27. ESI-TOF-MS of complex La_4L_2 with the observed and simulated isotopic patterns of the peaks corresponding to $[\text{La}_4\text{L}_2(\text{OTf})_8]^{4+}$.

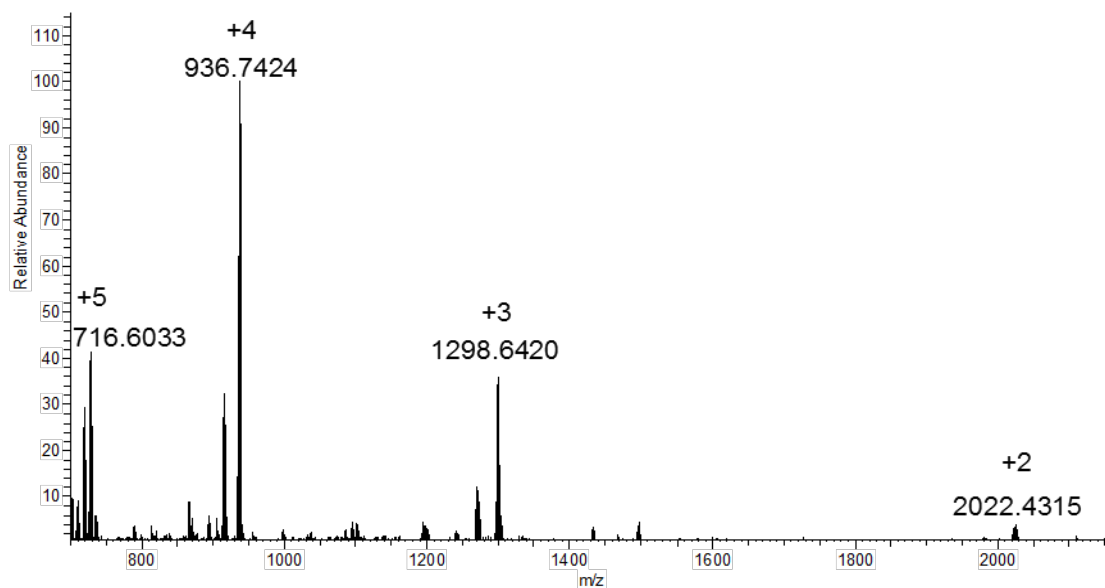


Figure S28. ESI-TOF-MS of complex Nd_4L_2 .

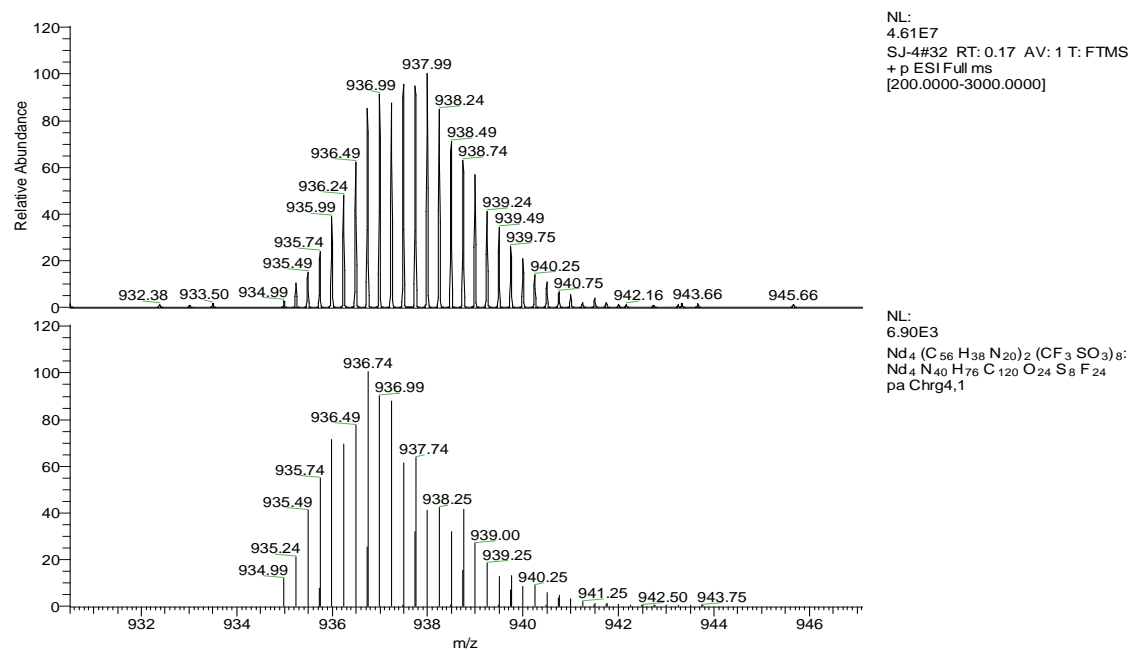


Figure S29. ESI-TOF-MS of complex Nd_4L_2 with the observed and simulated isotopic patterns of the peaks corresponding to $[\text{Nd}_4\text{L}_2(\text{OTf})_8]^{4+}$.

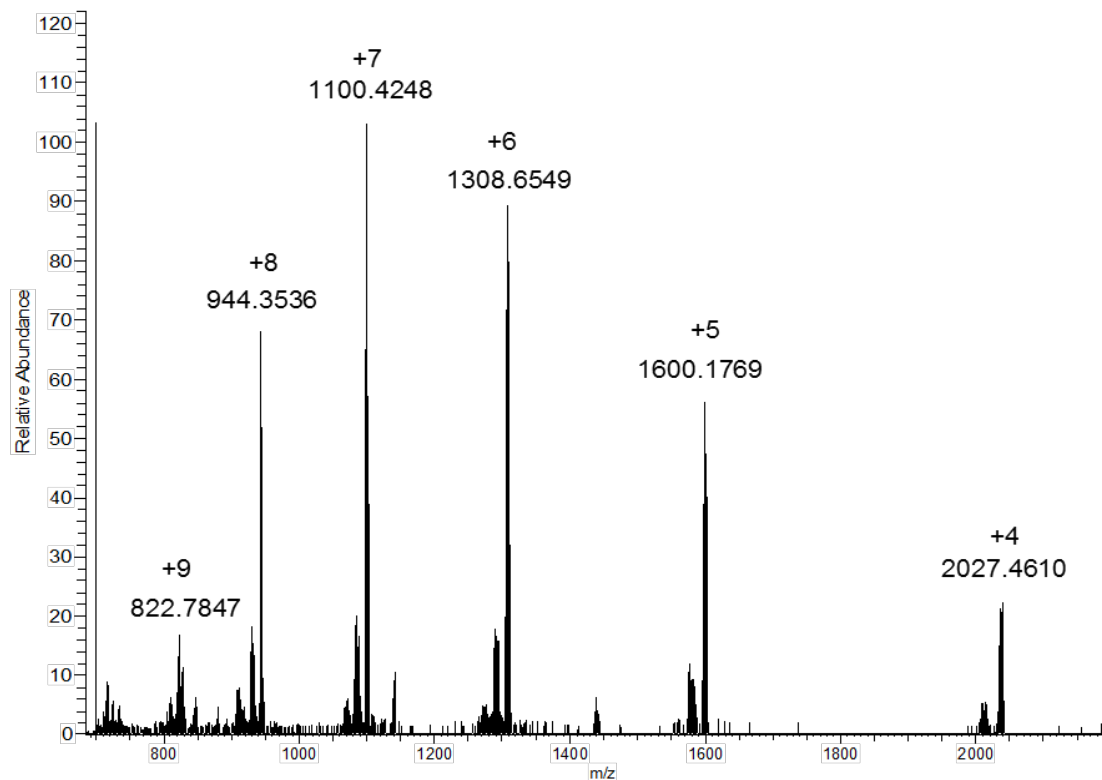


Figure S30. ESI-TOF-MS of complex Sm_8L_4 .

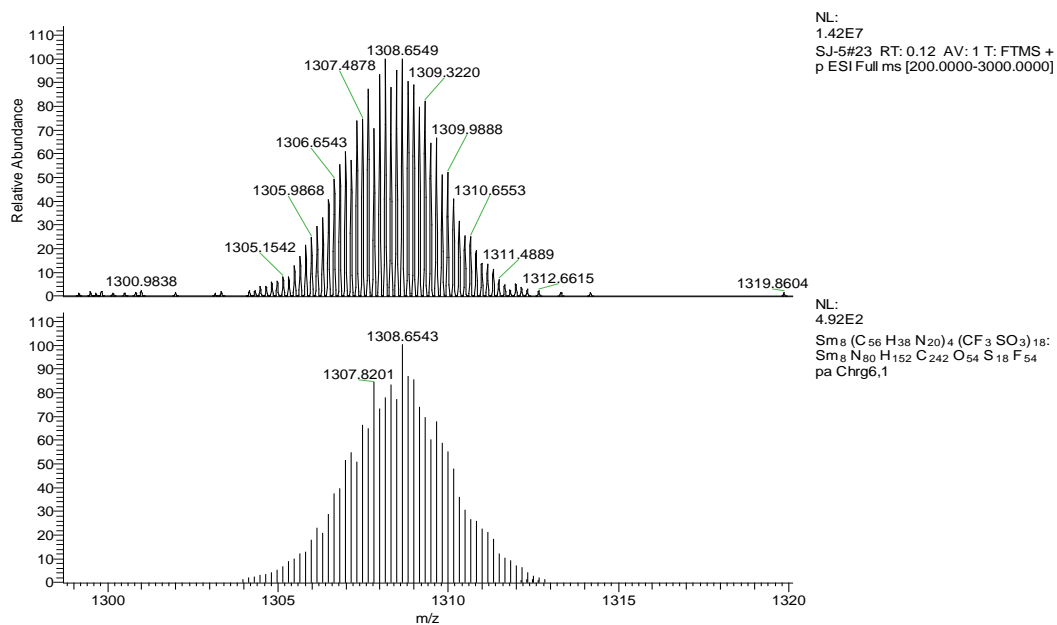


Figure S31. ESI-TOF-MS of complex Sm_8L_4 with the observed and simulated isotopic patterns of the peaks corresponding to $[\text{Sm}_8\text{L}_4(\text{OTf})_{18}]^{6+}$.

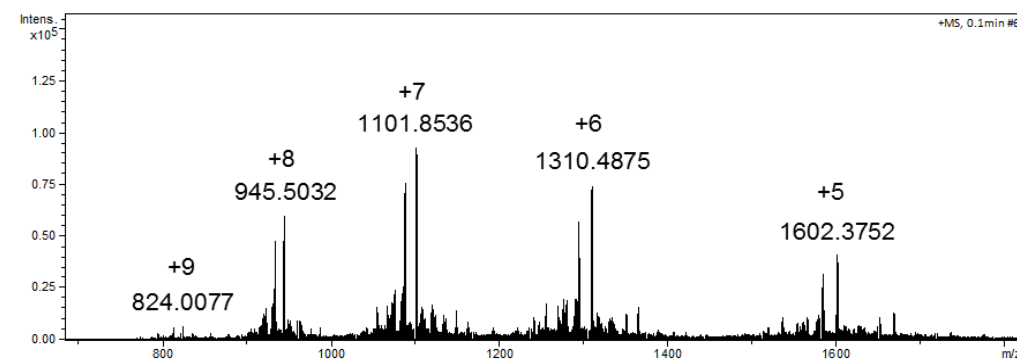


Figure S32. ESI-TOF-MS of complex Eu_8L_4 .

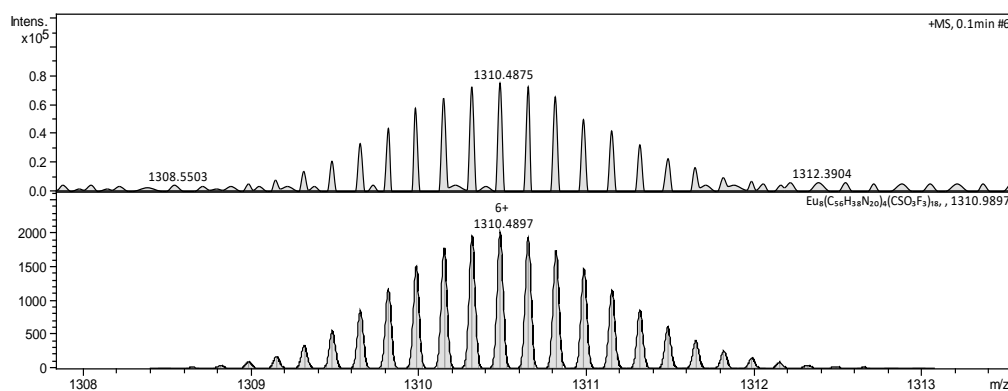


Figure S33. ESI-TOF-MS of complex Eu_8L_4 with the observed and simulated isotopic patterns of the peaks corresponding to $[\text{Eu}_8\text{L}_4(\text{OTf})_{18}]^{6+}$.

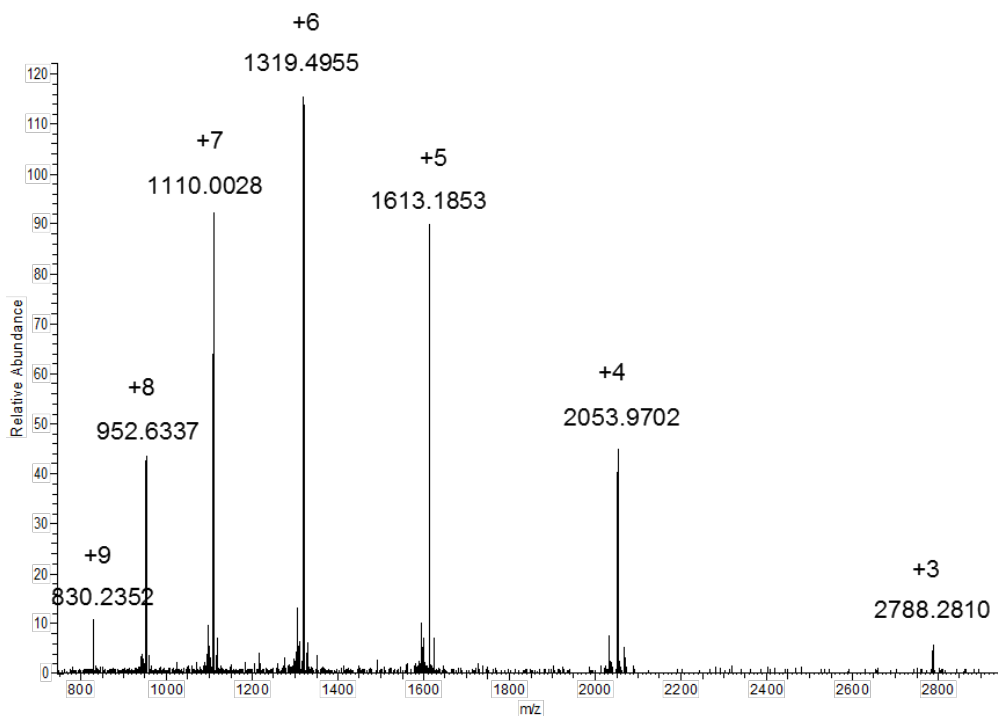


Figure S34. ESI-TOF-MS of complex Tb_8L_4 .

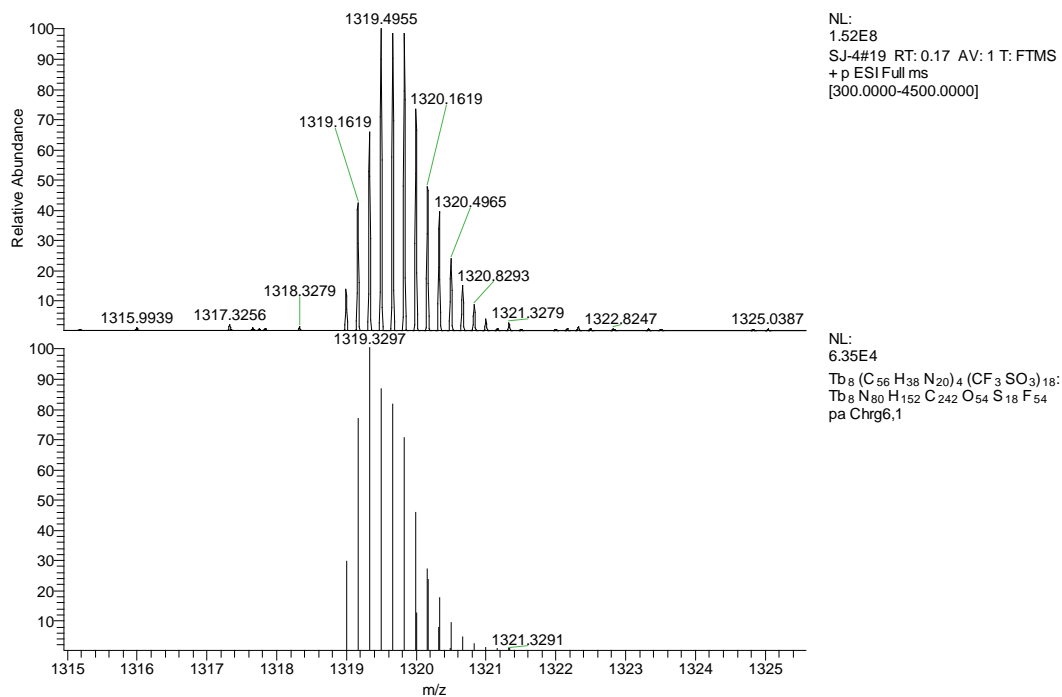


Figure S35. ESI-TOF-MS of complex Tb₈L₄ with the observed and simulated isotopic patterns of the peaks corresponding to [Tb₈L₄(OTf)₁₈]⁶⁺.

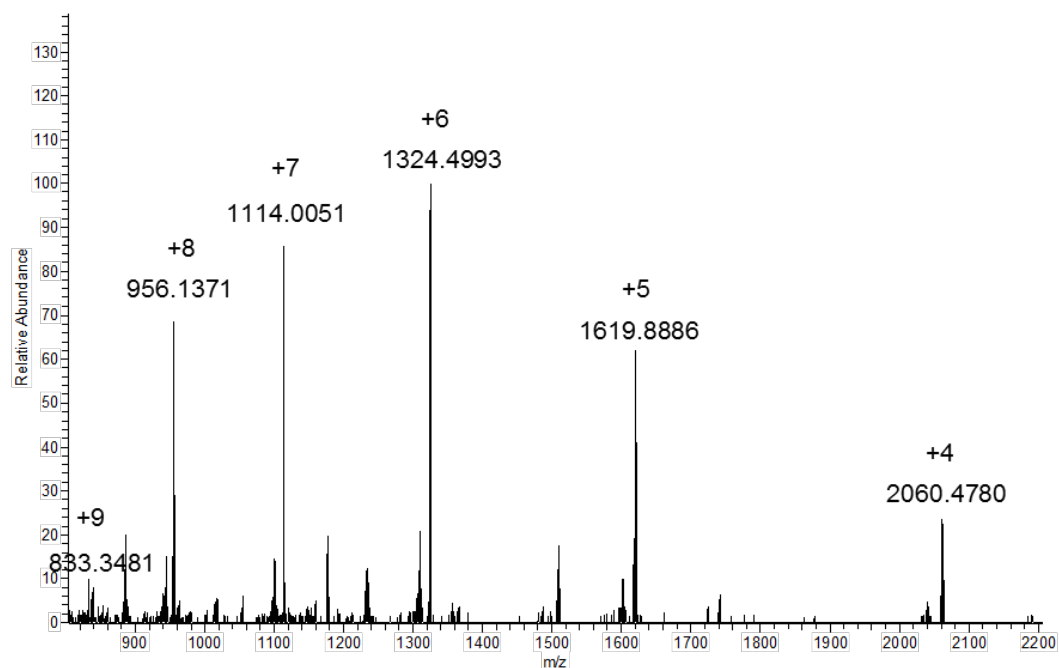


Figure S36. ESI-TOF-MS of complex Dy₈L₄.

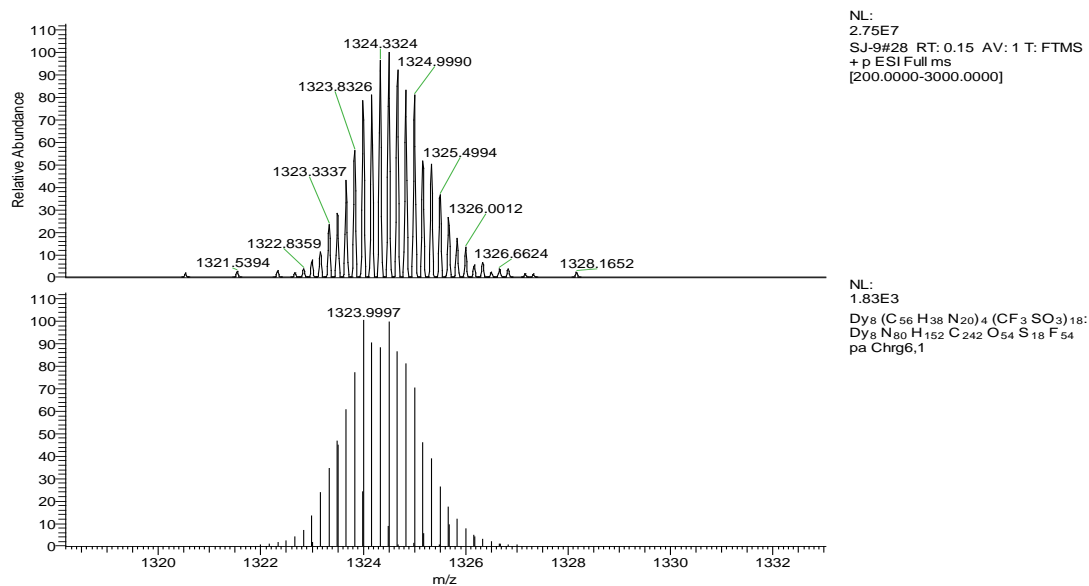


Figure S37. ESI-TOF-MS of complex Dy_8L_4 with the observed and simulated isotopic patterns of the peaks corresponding to $[\text{Dy}_8\text{L}_4(\text{OTf})_{18}]^{6+}$.

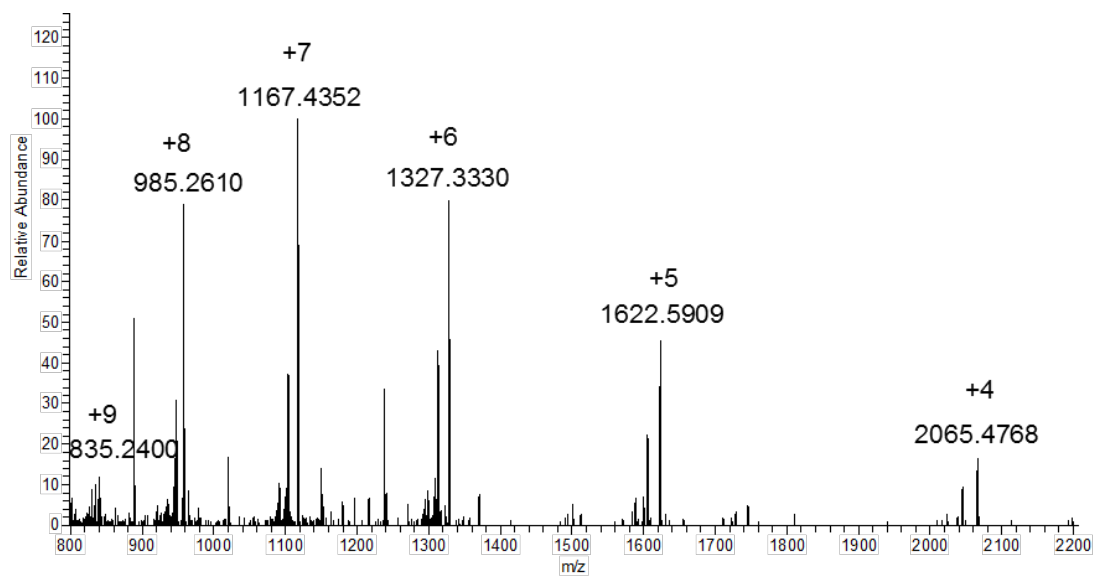


Figure S38. ESI-TOF-MS of complex Ho_8L_4 .

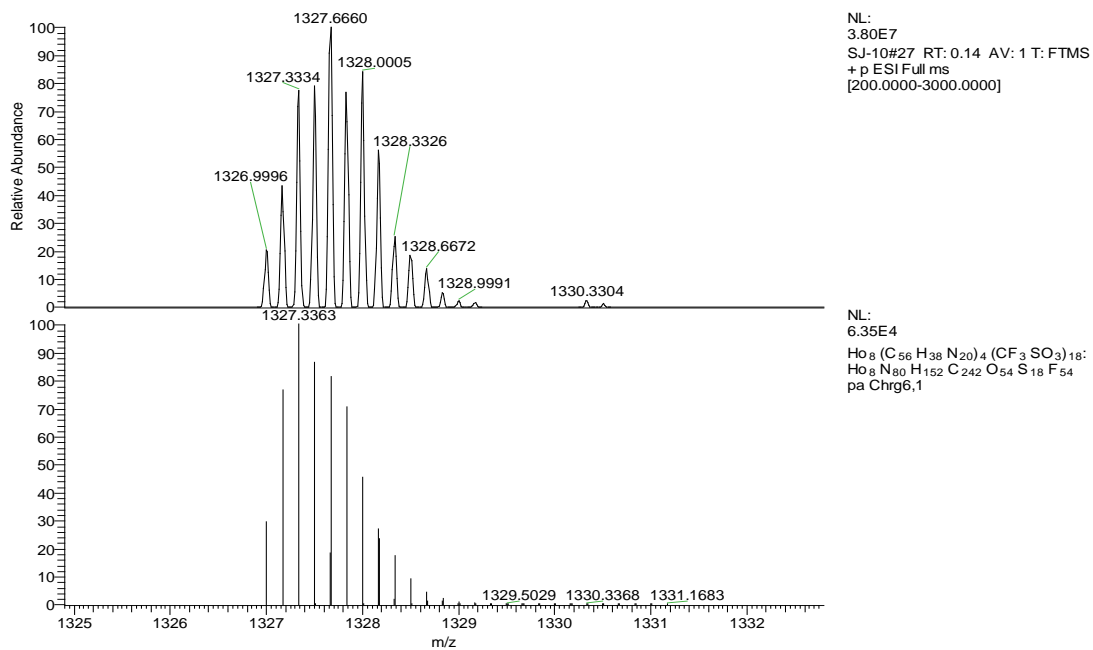


Figure S39. ESI-TOF-MS of complex Ho_8L_4 with the observed and simulated isotopic patterns of the peaks corresponding to $[\text{Ho}_8\text{L}_4(\text{OTf})_{18}]^{6+}$.

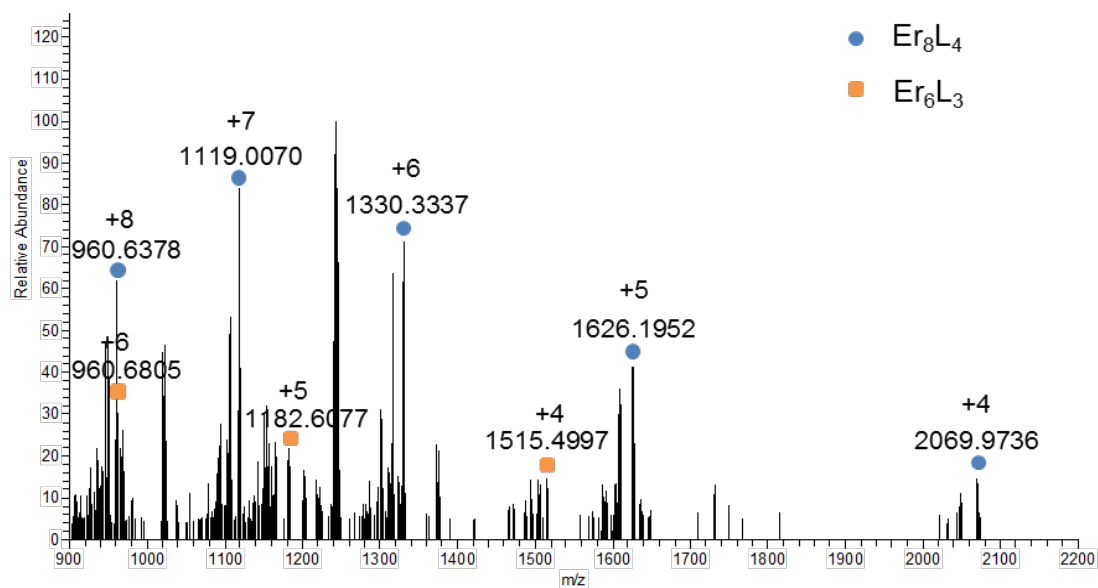


Figure S40. ESI-TOF-MS of complex Er_6L_3 and Er_8L_4 .

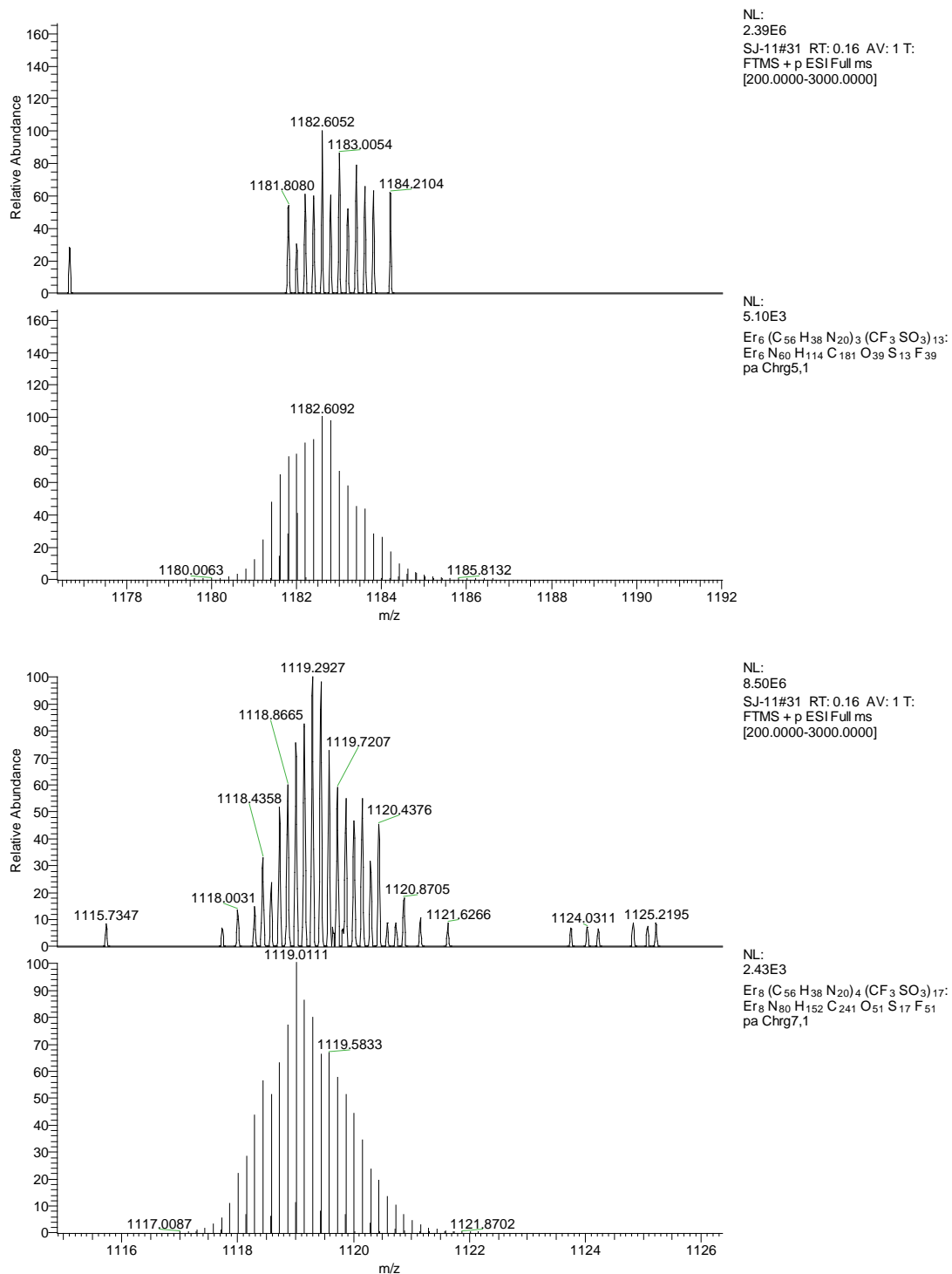


Figure S41. ESI-TOF-MS of complex Er₆L₃ and Er₈L₄ with the observed and simulated isotopic patterns of the peaks corresponding to [Er₆L₃(OTf)₁₃]⁵⁺ and [Er₈L₄(OTf)₁₇]⁷⁺.

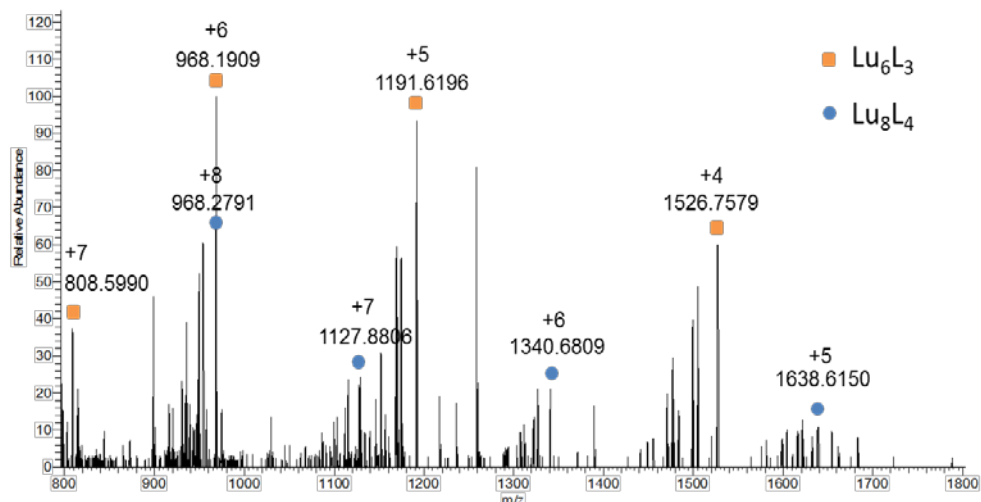


Figure S42. ESI-TOF-MS of complex Lu_6L_3 and Lu_8L_4 .

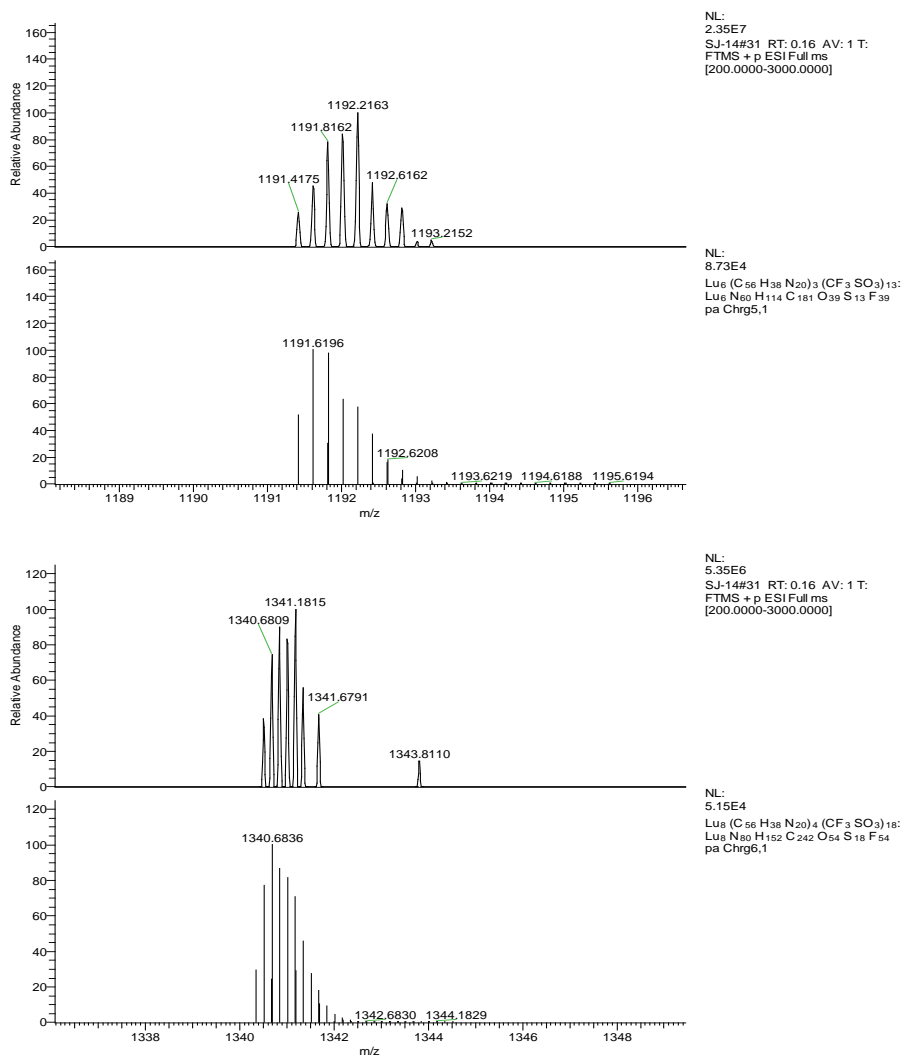


Figure S43. ESI-TOF-MS of complex Lu_6L_3 and Lu_8L_4 with the observed and simulated isotopic patterns of the peaks corresponding to $[\text{Lu}_6\text{L}_3(\text{OTf})_{13}]^{5+}$ (top) and $[\text{Lu}_8\text{L}_4(\text{OTf})_{18}]^{6+}$ (bottom), respectively.

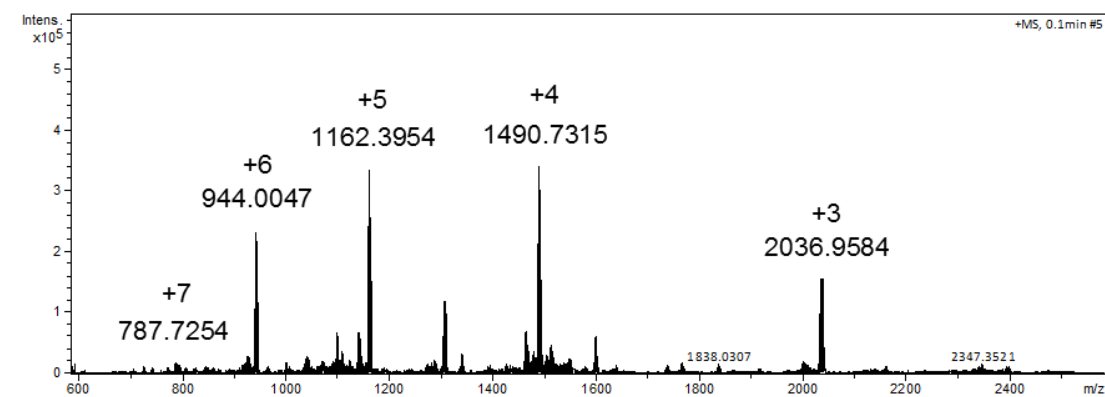


Figure S44. ESI-TOF-MS of complex Sm_6L_3 .

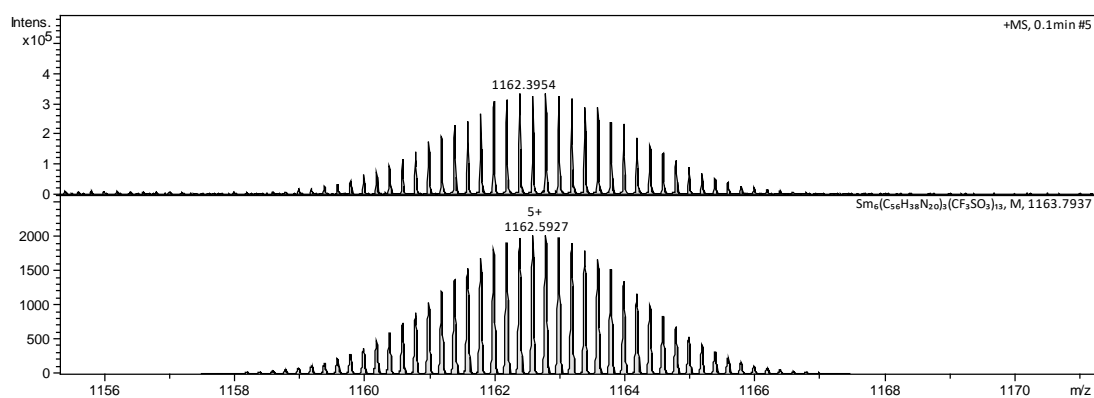


Figure S45. ESI-TOF-MS of complex Sm_6L_3 with the observed and simulated isotopic patterns of the peaks corresponding to $[\text{Sm}_6\text{L}_3(\text{OTf})_{13}]^{5+}$.

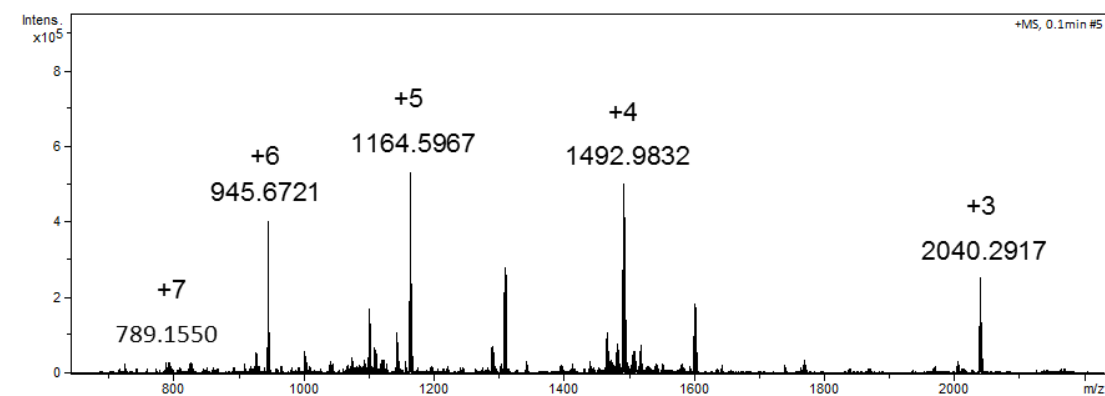


Figure S46. ESI-TOF-MS of complex Eu_6L_3 .

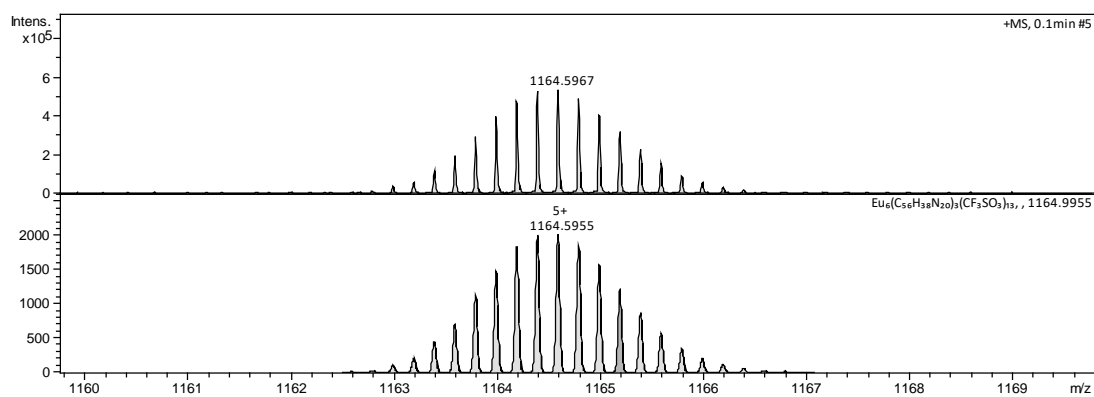


Figure S47. ESI-TOF-MS of complex Eu_6L_3 with the observed and simulated isotopic patterns of the peaks corresponding to $[\text{Eu}_6\text{L}_3(\text{OTf})_{13}]^{5+}$.

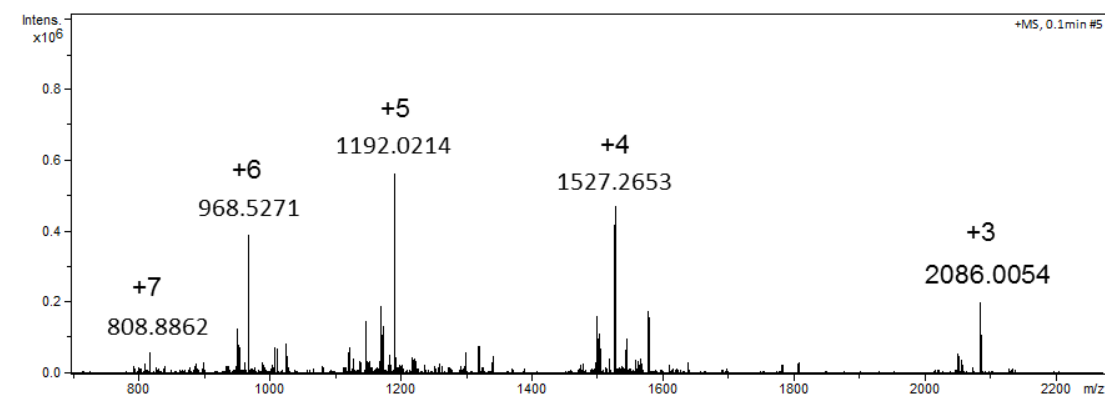


Figure S48. ESI-TOF-MS of complex Lu_6L_3 .

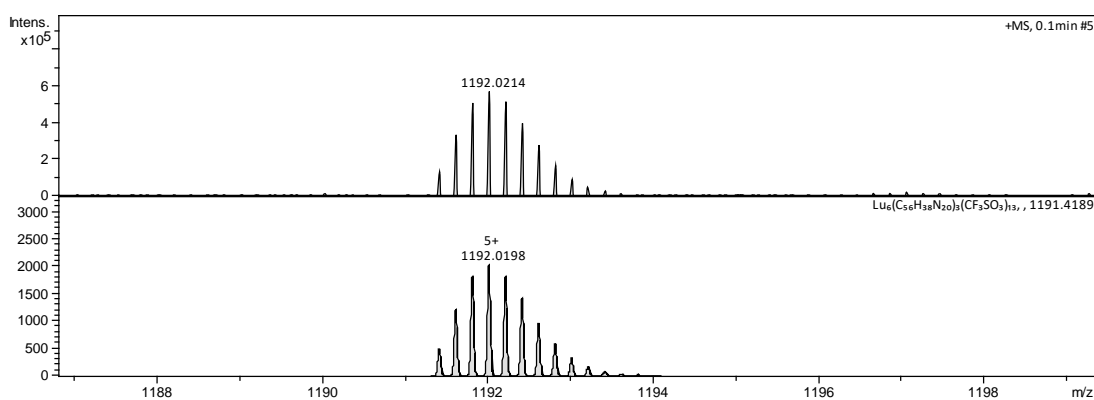


Figure S49. ESI-TOF-MS of complex Lu_6L_3 with the observed and simulated isotopic patterns of the peaks corresponding to $[\text{Lu}_6\text{L}_3(\text{OTf})_{13}]^{5+}$.

3. Single crystal X-ray diffraction studies

3.1 Crystal studies

Suitable single crystals of La_4L_2 were obtained by slow vapor diffusion of Et_2O into the acetonitrile solution of complexes at room temperature in a week. Single crystals of Sm_8L_4 and Tb_8L_4 were obtained by slow vapor diffusion THF into the acetonitrile solution of complexes at room temperature in two week. Single crystals of Ho_8L_4 were obtained by slow vapor diffusion EA into the acetonitrile solution of complexes at room temperature in two week. The X-ray diffraction for the crystals of La_4L_2 and Sm_8L_4 were carried out on micro-focus metal jet diffractometer using Ga $K\alpha$ radiation ($\lambda = 1.3405 \text{ \AA}$). The X-ray diffraction for the crystals of Tb_8L_4 and Ho_8L_4 were carried out on Bruker D8 VENTURE photon II diffractometer with $\text{I}\mu\text{s}$ 3.0 micro focus X-ray source using Mo $K\alpha$ radiation ($\lambda = 0.71073 \text{ \AA}$). All the collected diffraction data reductions were performed with the APEX-III software or the CrysAlisPro package. All structures were solved by direct methods and refined by full-matrix least-squares on F2 with anisotropic displacement using the Olex2 software package.² Solvent molecules and a portion of counter-ions in the unit cell were highly disordered and could not be reasonably located. These residual electron intensities were removed by PLATON/SQUEEZE routine.³ Details on crystal data collection and refinement were summarized in Table S1–S2.

Crystallographic data for La_4L_2 : Cubic space group $P2_1/n$, $a = 28.7537(6) \text{ \AA}$, $b = 29.1048(16) \text{ \AA}$, $c = 36.8307(10) \text{ \AA}$, $\alpha = \gamma = 90^\circ$, $\beta = 95.712(2)^\circ$, $V = 30669 \text{ \AA}^3$, $Z = 4$, $T = 293 \text{ K}$. Anisotropic least – squares refinement on 18025 independent merged reflections ($R_{\text{int}} = 0.1324$), converged at residual $wR_2 = 0.2798$ for all data; residual $R_1 = 0.0975$ for 13461 observed data [$I > 2\sigma(I)$], and goodness of fit (GOF) = 1.155.

Crystallographic data for Sm_8L_4 : Cubic space group $I4/m$, $a = b = 33.1015(4)$, $c = 52.4591(12) \text{ \AA}$, $\alpha = \beta = \gamma = 90^\circ$, $V = 57479.9(19) \text{ \AA}^3$, $Z = 4$, $T = 100 \text{ K}$. Anisotropic least–squares refinement on 9189 independent merged reflections ($R_{\text{int}} = 0.0504$), converged at residual $wR_2 = 0.2610$ for all data; residual $R_1 = 0.0923$ for 7754 observed

data [$I > 2\sigma(I)$], and goodness of fit (GOF) = 1.015.

Crystallographic data for Tb₈L₄: Cubic space group $I4/m$, $a = b = 33.1128(5)$, $c = 52.648(2)$ Å, $\alpha = \beta = \gamma = 90^\circ$, $V = 57726(3)$ Å³, $Z = 4$, $T = 100$ K. Anisotropic least – squares refinement on 8681 independent merged reflections ($R_{\text{int}} = 0.0650$), converged at residual $wR_2 = 0.2907$ for all data; residual $R_1 = 0.1120$ for 7195 observed data [$I > 2\sigma(I)$], and goodness of fit (GOF) = 1.056.

Crystallographic data for Ho₈L₄: Cubic space group $I4/m$, $a = b = 33.4347(3)$, $c = 54.6188(10)$ Å, $\alpha = \beta = \gamma = 90^\circ$, $V = 61057.2(16)$ Å³, $Z = 4$, $T = 279$ K. Anisotropic least – squares refinement on 26422 independent merged reflections ($R_{\text{int}} = 0.0398$), converged at residual $wR_2 = 0.1783$ for all data; residual $R_1 = 0.0518$ for 16827 observed data [$I > 2\sigma(I)$], and goodness of fit (GOF) = 0.996.

Table S1. Crystallographic data for La₄L₂ and Sm₈L₄.

Identification code	La ₄ L ₂	Sm ₈ L ₄
Empirical formula	C ₁₂₁ H ₉₀ F ₂₇ La ₄ N ₄₀ O ₃₄ S ₉	C ₂₅₆ H ₂₀₀ F ₄₈ N ₈₀ O ₆₀ S ₁₆ Sm ₈
Formula weight	4005.50	7984.71
Temperature/K	293	100
Crystal system	monoclinic	tetragonal
Space group	$P2_1/n$	$I4/m$
$a/\text{Å}$	28.7537(6)	33.1015(4)
$b/\text{Å}$	29.1048(16)	33.1015(4)
$c/\text{Å}$	36.8307(10)	52.4591(12)
$\alpha/^\circ$	90	90
$\beta/^\circ$	95.712(2)	90
$\gamma/^\circ$	90	90
Volume/Å ³	30669(2)	57479.9(19)
Z	4	4
$\rho_{\text{calc}}/\text{cm}^3$	0.867	0.923
μ/mm^{-1}	5.316	4.939
$F(000)$	7932.0	15840.0
Crystal size/mm ³	0.35 × 0.23 × 0.16	0.26 × 0.23 × 0.22
Radiation	Cu K α ($\lambda = 1.54184$)	Ga K α ($\lambda = 1.3405$)
2Θ range for data collection/ $^\circ$	4.822 to 79.942	4.97 to 69.898
Index ranges	$-23 \leq h \leq 22$, $-24 \leq k \leq 24$, $-25 \leq l \leq 30$	$-28 \leq h \leq 27$, $-20 \leq k \leq 28$, $-44 \leq l \leq 44$

Reflections collected	76296	37759
Independent reflections	18025 [R _{int} = 0.1324, R _{sigma} = 0.0789]	9189 [R _{int} = 0.0504, R _{sigma} = 0.0312]
Data/restraints/parameters	18025/2451/2146	9189/3007/1102
Goodness-of-fit on F²	1.155	1.015
Final R indexes [I ≥ 2σ (I)]	R ₁ = 0.0975, wR ₂ = 0.2619	R ₁ = 0.0923, wR ₂ = 0.2461
Final R indexes [all data]	R ₁ = 0.1119, wR ₂ = 0.2798	R ₁ = 0.1037, wR ₂ = 0.2610
Largest diff. peak/hole / e Å⁻³	0.90/-1.09	1.49/-0.86

Table S2. Crystallographic data for Tb₈L₄ and Ho₈L₄.

Identification code	Tb ₈ L ₄	Ho ₈ L ₄
Empirical formula	C ₂₅₆ H ₂₀₀ F ₄₈ N ₈₀ O ₆₀ S ₁₆ Tb ₈	C ₂₄₀ H ₁₇₆ F ₄₈ Ho ₈ N ₈₀ O ₆₀ S ₁₆
Formula weight	8053.27	7885.00
Temperature/K	100	279
Crystal system	tetragonal	tetragonal
Space group	<i>I4/m</i>	<i>I4/m</i>
a/Å	33.1128(5)	33.4347(3)
b/Å	33.1128(5)	33.4347(3)
c/Å	52.648(2)	54.6188(10)
α/°	90	90
β/°	90	90
γ/°	90	90
Volume/Å³	57726(3)	61057.2(16)
Z	4	4
ρ_{calc}/cm³	0.927	0.858
μ/mm⁻¹	1.086	1.136
F(000)	15936.0	15520.0
Crystal size/mm³	0.2 × 0.15 × 0.15	0.31 × 0.22 × 0.22
Radiation	Mo Kα (λ = 0.71073)	Mo Kα (λ = 0.71073)
2θ range for data collection/°	3.77 to 34.45	3.524 to 50.054
Index ranges	-26 ≤ h ≤ 27, -26 ≤ k ≤ 27, -43 ≤ l ≤ 43	-39 ≤ h ≤ 39, -39 ≤ k ≤ 36, -65 ≤ l ≤ 62
Reflections collected	38394	88098
Independent reflections	8681 [R _{int} = 0.0650, R _{sigma} = 0.0341]	26422 [R _{int} = 0.0398, R _{sigma} = 0.0425]
Data/restraints/parameters	8681/2722/1040	26422/3840/1020

Goodness-of-fit on F²	1.056	0.996
Final R indexes [I>=2σ (I)]	R ₁ = 0.1120, wR ₂ = 0.2756	R ₁ = 0.0518, wR ₂ = 0.1565
Final R indexes [all data]	R ₁ = 0.1294, wR ₂ = 0.2907	R ₁ = 0.0799, wR ₂ = 0.1783
Largest diff. peak/hole / e Å⁻³	1.24/-1.27	1.18/-0.64

Table S3. SHAPE Analysis for the La₄L₂ coordination sphere.

	DP-10	EPY-10	OBPY-10	PPR-10	PAPR-10
	D _{10h}	C _{9v}	D _{8h}	D _{5h}	D _{5d}
La1	33.55514	24.34721	18.45960	10.54960	13.19975
La2	33.77836	24.57340	18.55938	10.43711	13.36656
La3	34.12318	23.95758	18.64400	10.83278	13.13226
La4	33.43324	24.05756	18.60198	10.73882	13.42397
	JBCCU-10	JBCSAPR-10	JMBIC-10	JATDI-10	JSPC-10
	D _{4h}	D _{4d}	C _{2v}	C _{3v}	C _{2v}
La1	9.36561	1.92703	8.38762	18.58957	2.64771
La2	9.79330	2.09502	8.66815	18.02310	2.61702
La3	9.51433	2.08036	8.20928	17.93841	2.64442
La4	9.46504	1.94334	8.68037	18.14712	2.80262
	SDD-10	TD-10	HD-10		
	D ₂	C _{2v}	D _{4h}		
La1	5.94404	5.48180	8.27688		
La2	6.42828	5.62447	8.56720		
La3	6.40099	5.07362	8.30166		
La4	6.24939	5.63370	8.39848		

Table S4. SHAPE Analysis for the Sm₈L₄ coordination sphere.

	EP-9	OPY-9	HBPY-9	JTC-9	JCCU-9
	D _{9h}	C _{8v}	D _{7h}	C _{3v}	C _{4v}
Sm1	34.76975	23.45528	18.88305	14.45895	10.32630
Sm2	34.70755	23.30092	18.24248	14.05970	9.82417
	CCU-9	JCSAPR-9	CSAPR-9	JTCTPR-9	TCTPR-9
	C _{4v}	C _{4v}	C _{4v}	D _{3h}	D _{3h}
Sm1	8.67011	2.05377	1.25807	2.19146	1.13979

Sm2	8.82192	1.63352	0.81384	2.52308	1.40294
	JTDIC-9	HH-9	MFF-9		
	C _{3v}	C _{2v}	C _s		
Sm1	11.17981	11.11199	1.85508		
Sm2	11.39006	10.43420	1.26745		

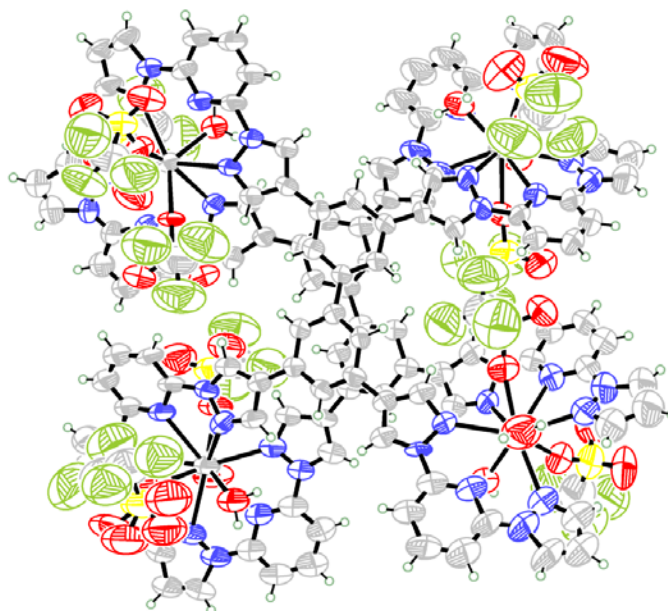


Figure S50. Ortep-drawing of the asymmetric unit in the crystal structure of La₄L₂ at 50% probability level.

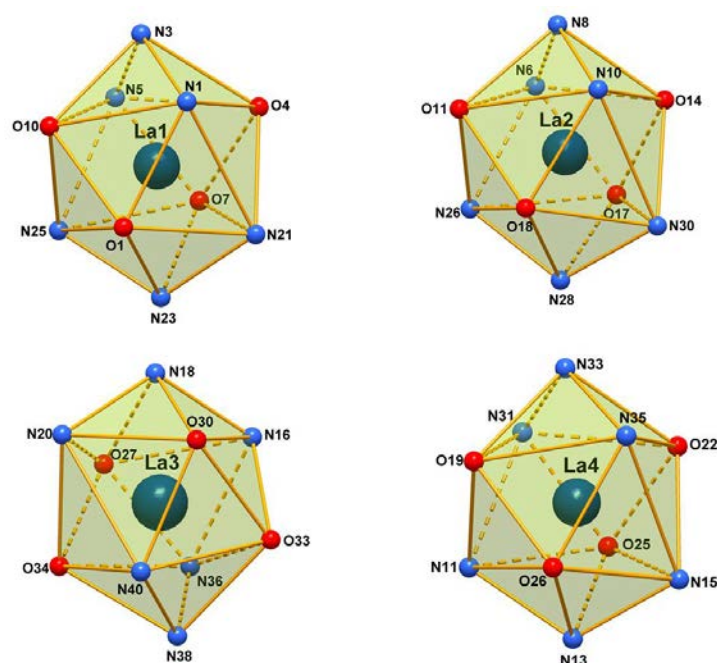


Figure S51. The coordination geometry for La1, La2, La3 and La4 in La₄L₂.

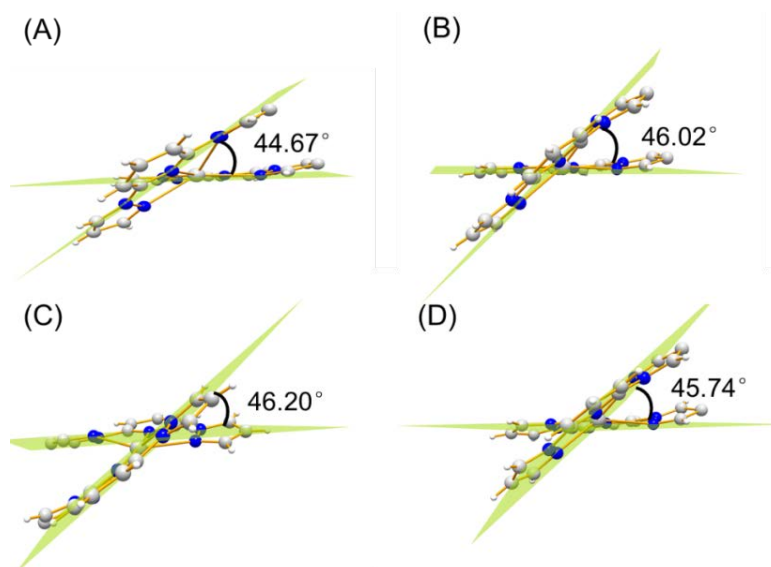


Figure S52. The dihedral angles between metal-chelating planes around the La^{3+} node in La_4L_2 : (A) La1, (B) La2, (C) La3, (D) La4.

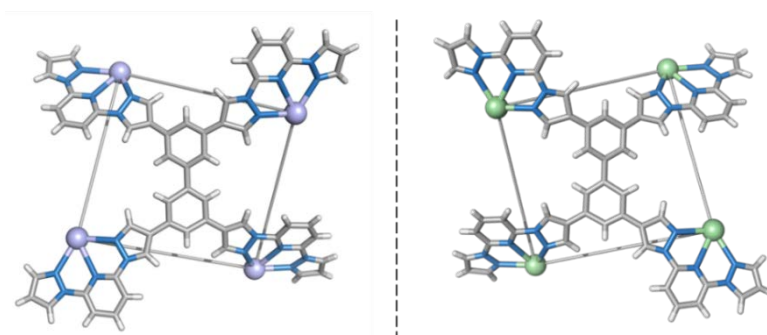


Figure S53. Metal-centered configurations of La_4L_2 (green: Δ ; purple: Λ).

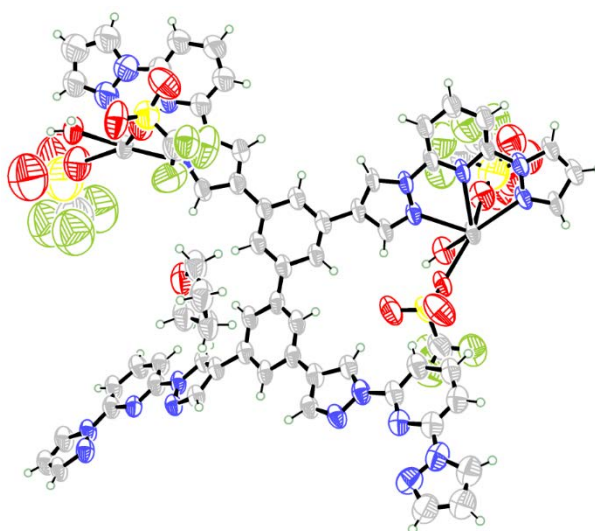


Figure S54. Ortep-drawing of the asymmetric unit in the crystal structure of Sm_8L_4 at 50% probability level.

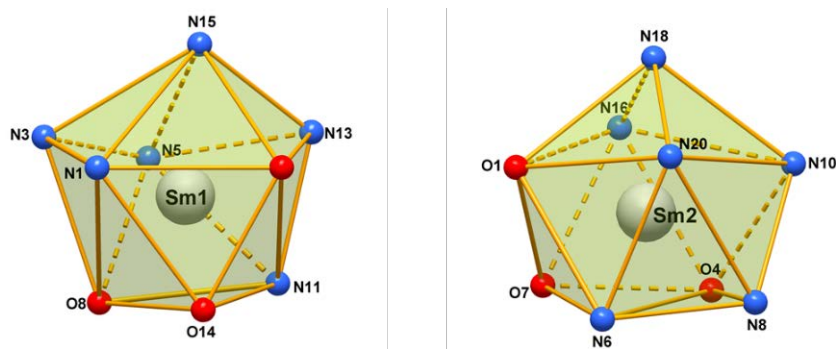


Figure S55. The coordination geometry for Sm1 and Sm2 in Sm_8L_4 .

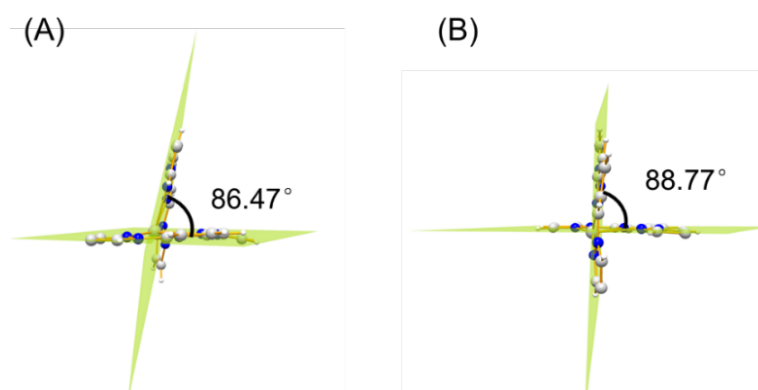


Figure S56. The dihedral angles between metal-chelating planes around the Sm^{3+} node in Sm_8L_4 : (A) Sm1, (B) Sm2.

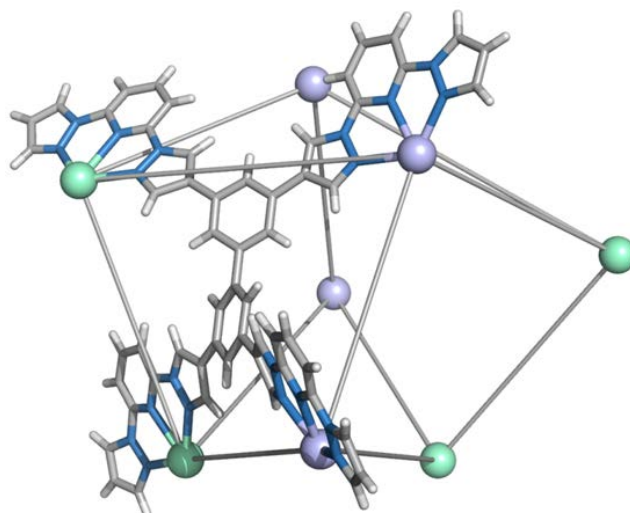


Figure S57. Metal-centered configurations of Sm_8L_4 (green: Δ ; purple: Λ).

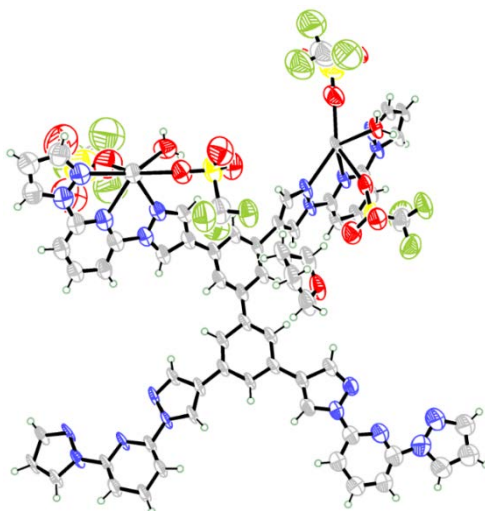


Figure S58. Ortep-drawing of the asymmetric unit in the crystal structure of Tb₈L₄ at 50% probability level.

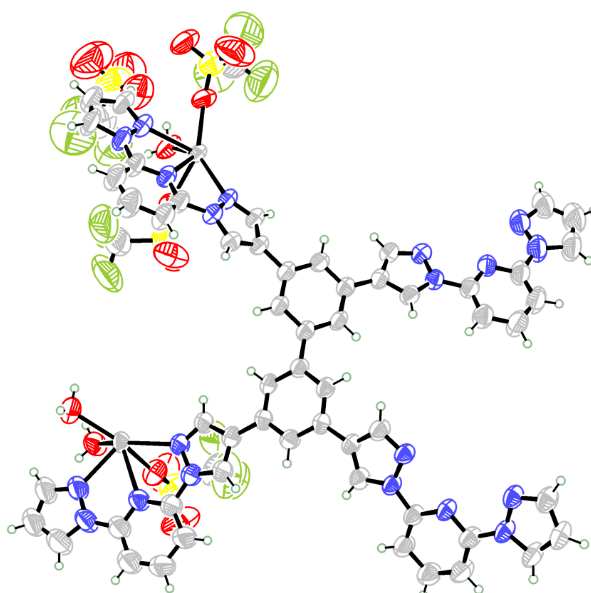


Figure S59. Ortep-drawing of the asymmetric unit in the crystal structure of Ho₈L₄ at 50% probability level.

3.2 Volume calculations

Cavity volumes of Sm₈L₄ was calculated by MoloVol based on their crystal structures after omitting the encapsulated guests.⁴ The related parameters were used in the calculations as follow:

Probe mode: one probe

Probe radius: 1.4 Å

Volume: 594.521 Å³

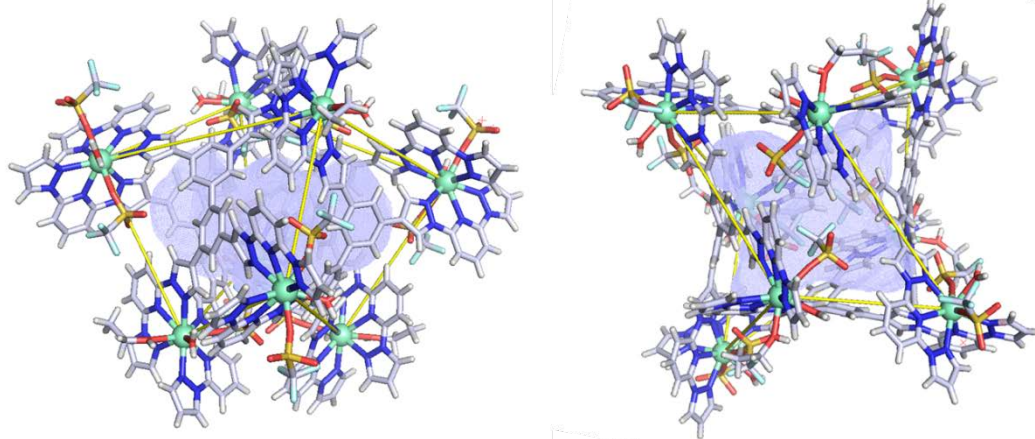


Figure S60. The view of calculated cavity volume of Sm₈L₄.

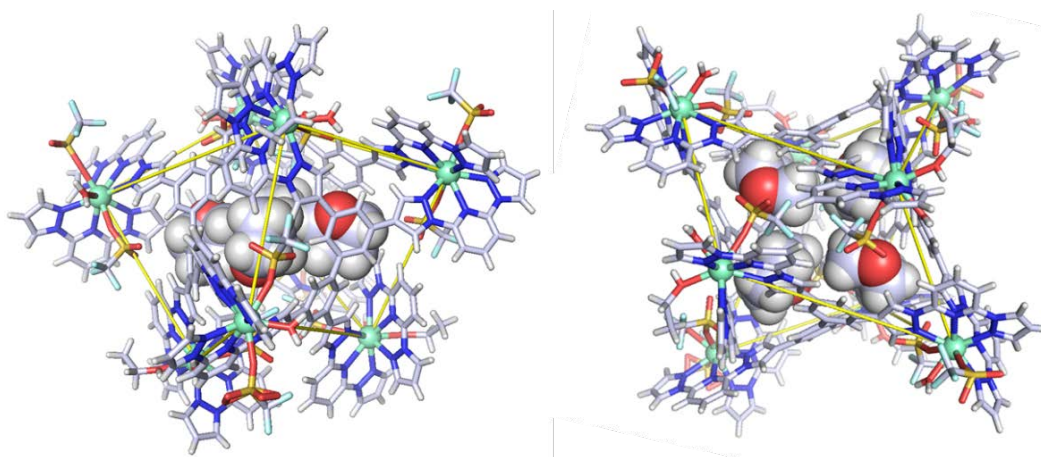


Figure S61. Crystal Structure of Sm₈L₄ Host-guest Complex.

4. Host-guest studies

4.1 General procedure for host-guest studies

In the process of processing crystal data, it was discovered that four tetrahydrofuran molecules encapsulated in the Sm_8L_4 structure. Therefore, an excess of the guest (10 equivalents) was added to Sm_8L_4 (0.001 mmol) in CD_3CN , and then heated at 70°C for 30 minutes to prepare the host-guest complex. To estimate the associate constants, the NMR titration experiments were also carried out and the experimental processes of them were as follows: the guest tetrahydrofuran molecule is diluted in an acetonitrile solution (0.031 M), and then added into the Sm_8L_4 host (0.0025 M, 400 μL CD_3CN) to perform the titration experiments.

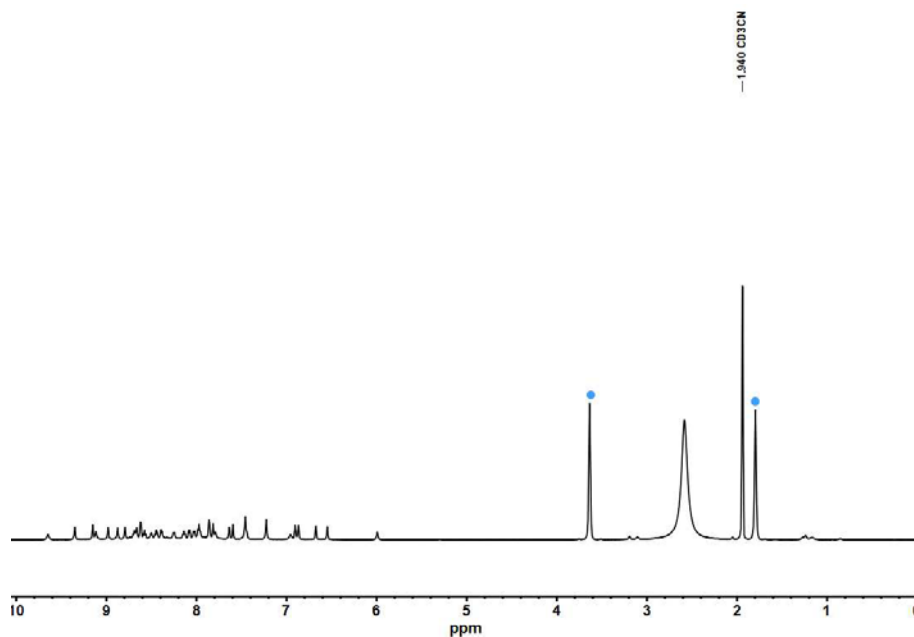


Figure S62. ^1H NMR spectra of Sm_8L_4 host-guest complexes. (An excess of guests was added, 400 MHz, CD_3CN , 298 K).

4.2 Binding constants estimation

The binding behavior of cage Sm_8L_4 for guests have been estimated by ^1H NMR titrations and fitted with a Hill function:

$$\log \frac{\theta}{1 - \theta} = n \log[G] + n \log[K_a]$$

θ = saturated ratio

$\theta_i = \Delta\delta_i/\Delta\delta_{\max}$

n: Hill coefficient

[G]=concentration of guest

K_a = apparent association constant

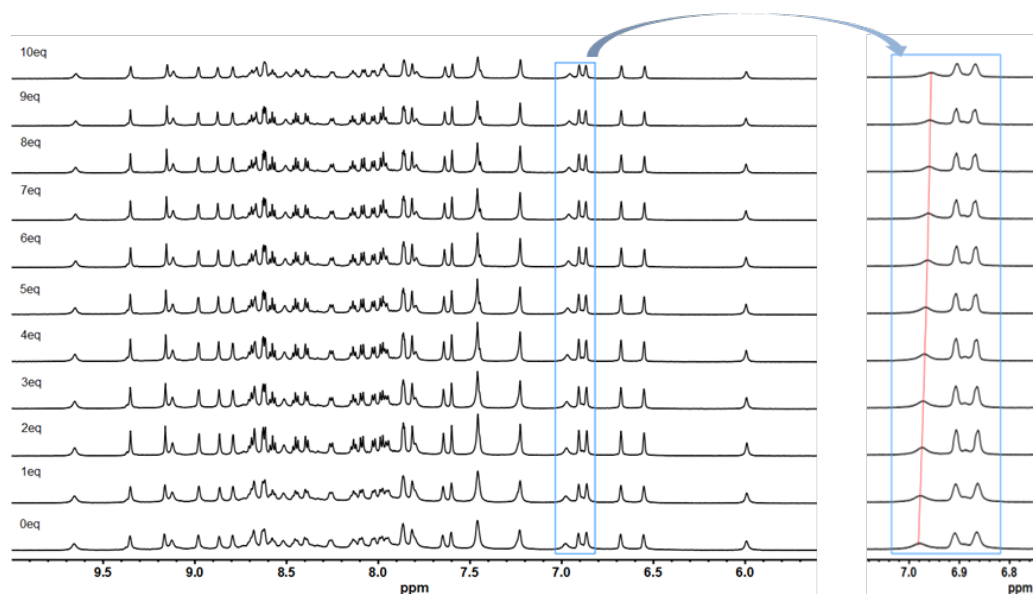


Figure S63. ^1H NMR titration of Sm_8L_4 with THF. Conditions: $c(\text{Sm}_8\text{L}_4) = 0.0025 \text{ M}$, CD_3CN ($400 \mu\text{L}$), 400 MHz , 298 K .

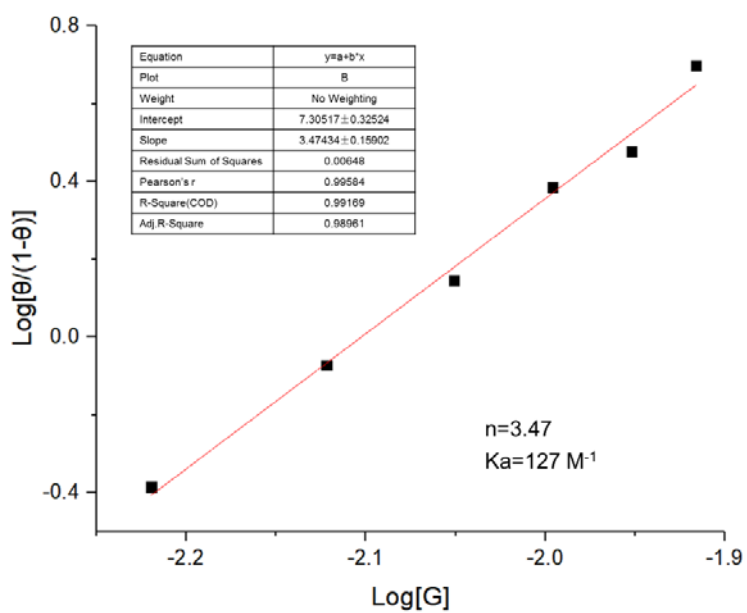
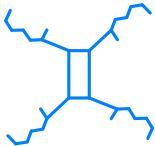
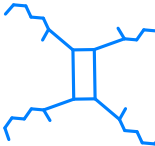
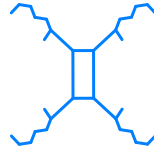
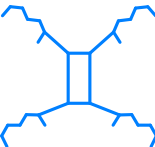
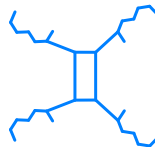
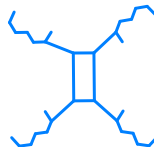
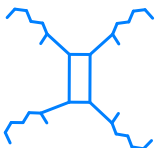
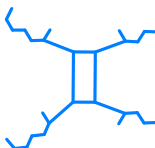
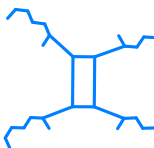


Figure S64. ^1H NMR titration of Sm_8L_4 with THF. Conditions: $c(\text{Sm}_8\text{L}_4) = 0.0025 \text{ M}$, CD_3CN ($400 \mu\text{L}$), 400 MHz , 298 K .

5. The rich conformations of the ligand L

Table S6. The nine conformations of ligand L.

Mode A	Mode B	Mode C
		
Mode D	Mode E	Mode F
		
Mode G	Mode H	Mode I
		

6. UV-Vis and FL spectra

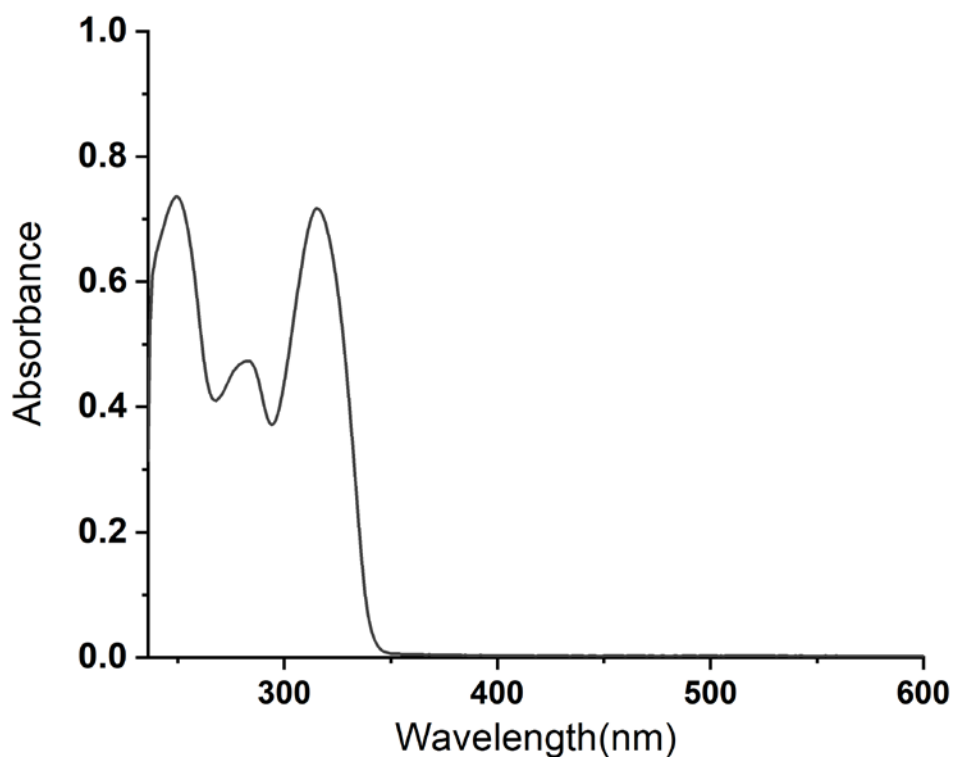


Figure S65. UV-vis spectra of **L** ($c = 1 \times 10^{-5}$ M, CH₃Cl).

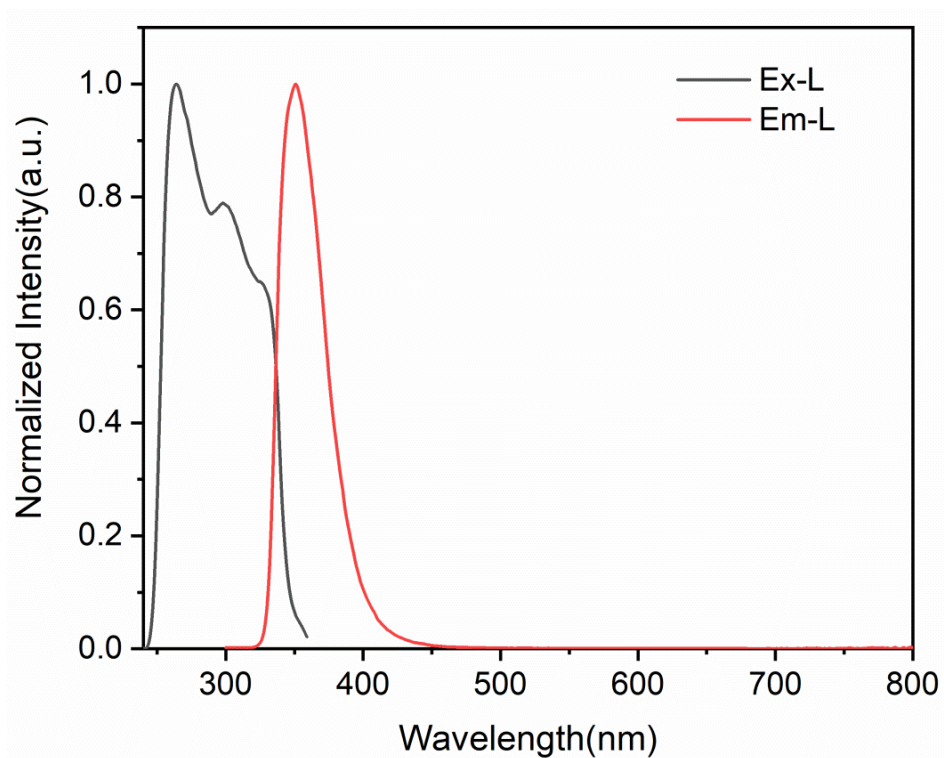


Figure S66. Excitation and emission spectra of **L** ($c = 1 \times 10^{-5}$ M, CH₃Cl).

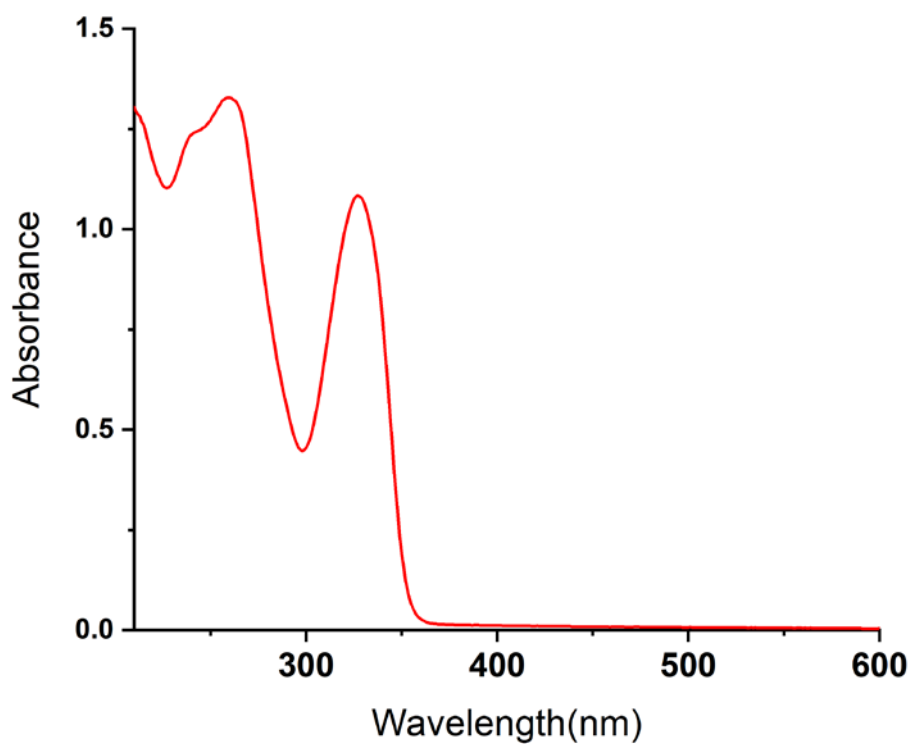


Figure S67. UV-vis spectra of Tb_8L_4 ($c = 1 \times 10^{-5}$ M, CH_3CN).

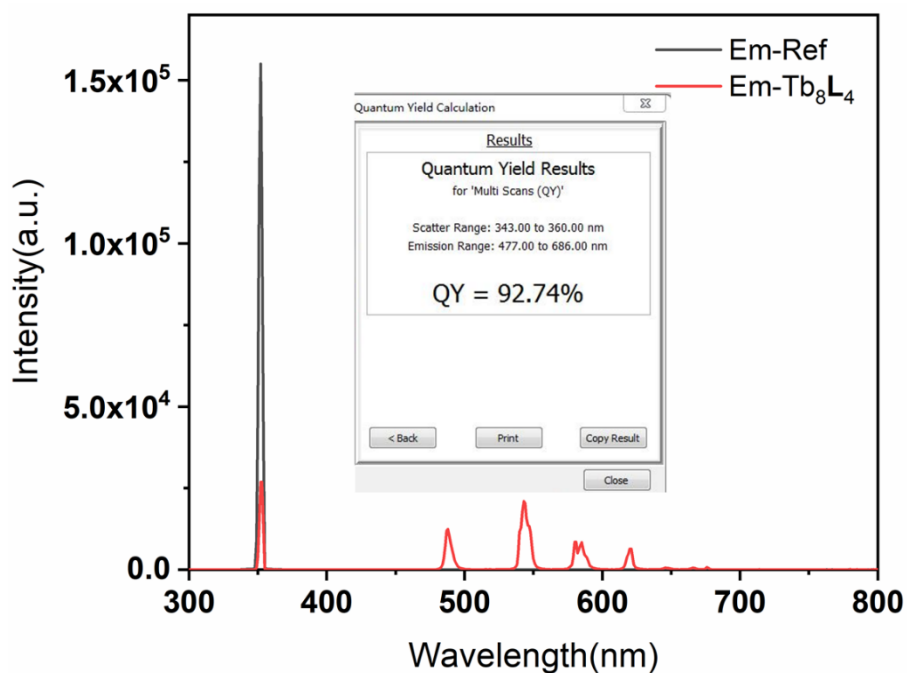


Figure S68. The superposition of emission spectra of reference and Tb_8L_4 ($\lambda_{\text{ex}} = 353$ nm, $c = 1 \times 10^{-5}$ M in CH_3CN , $\Phi_{\text{overall}} = 92.74\%$).

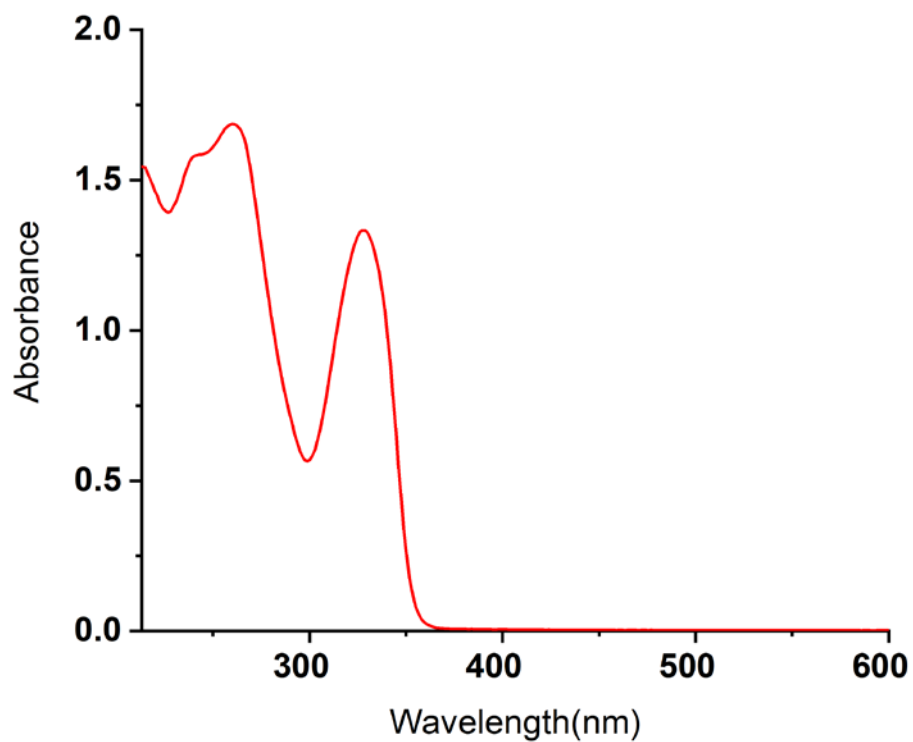


Figure S69. UV-vis spectra of Sm_8L_4 ($c = 1 \times 10^{-5}$ M, CH_3CN).

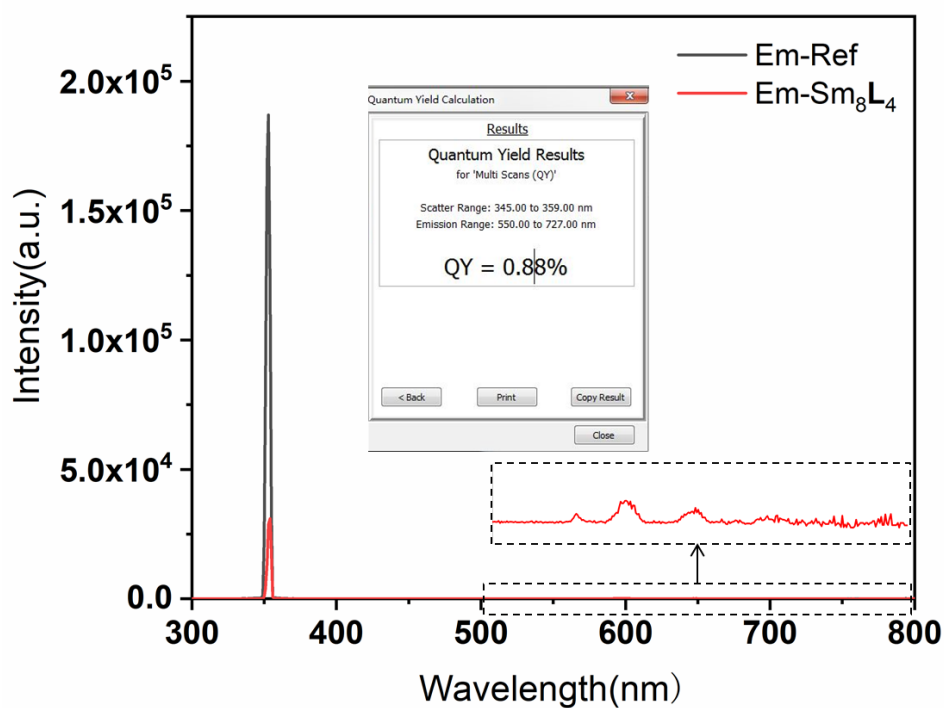


Figure S70. The superposition of emission spectra of reference and Sm_8L_4 ($\lambda_{\text{ex}} = 354$ nm, $c = 1 \times 10^{-5}$ M in CH_3CN , $\Phi_{\text{overall}} = 0.88\%$).

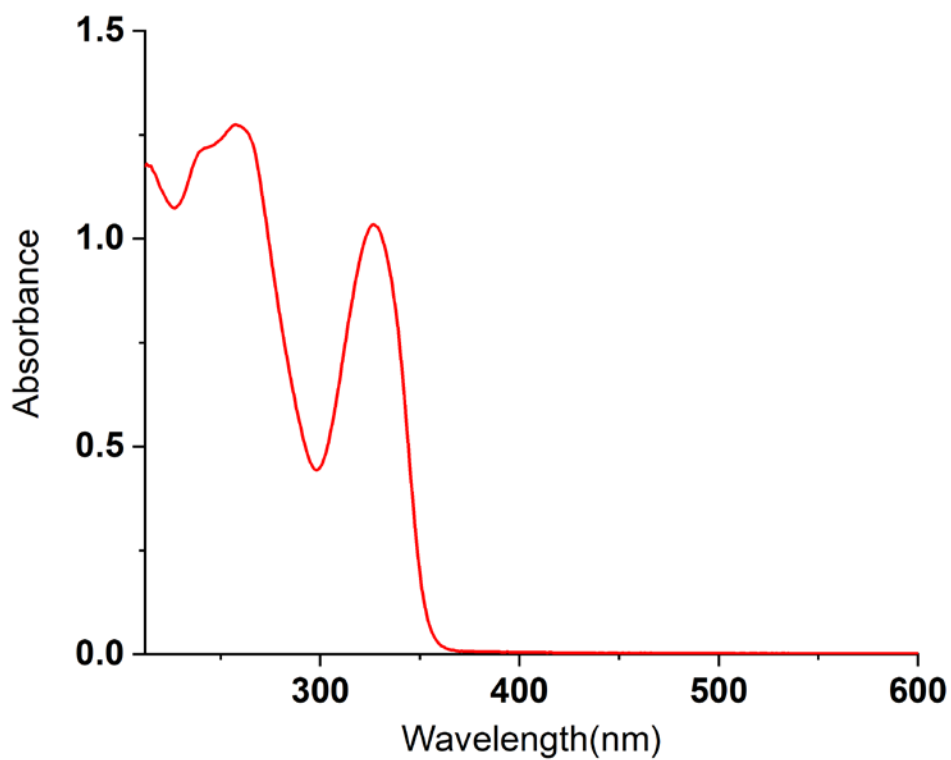


Figure S71. UV-vis spectra of Dy_8L_4 ($c = 1 \times 10^{-5}$ M, CH_3CN).

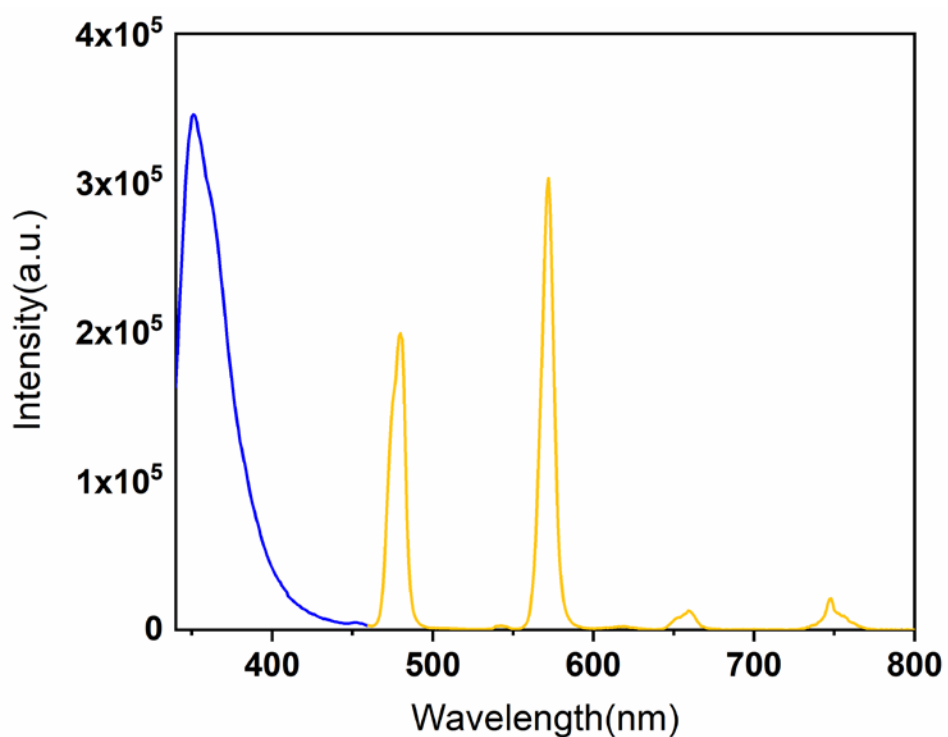


Figure S72. Emission spectra of Dy_8L_4 ($c = 1 \times 10^{-5}$ M, CH_3CN , $\lambda_{\text{ex}}=315\text{nm}$).

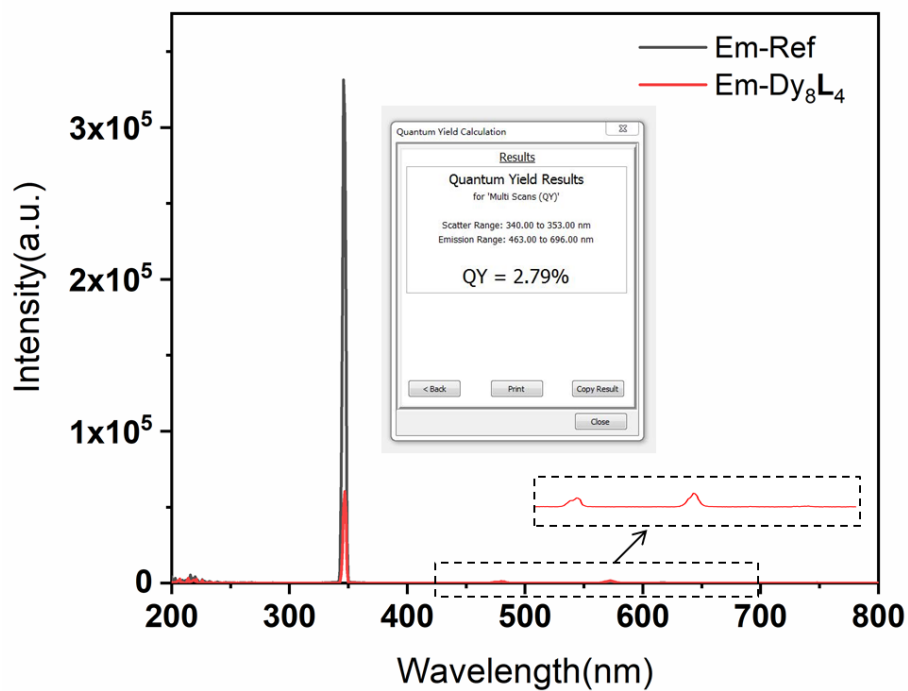


Figure S73. The superposition of emission spectra of reference and Dy_8L_4 ($\lambda_{\text{ex}} = 347$ nm, $c = 1 \times 10^{-5}$ M in CH_3CN , $\Phi_{\text{overall}} = 2.79\%$).

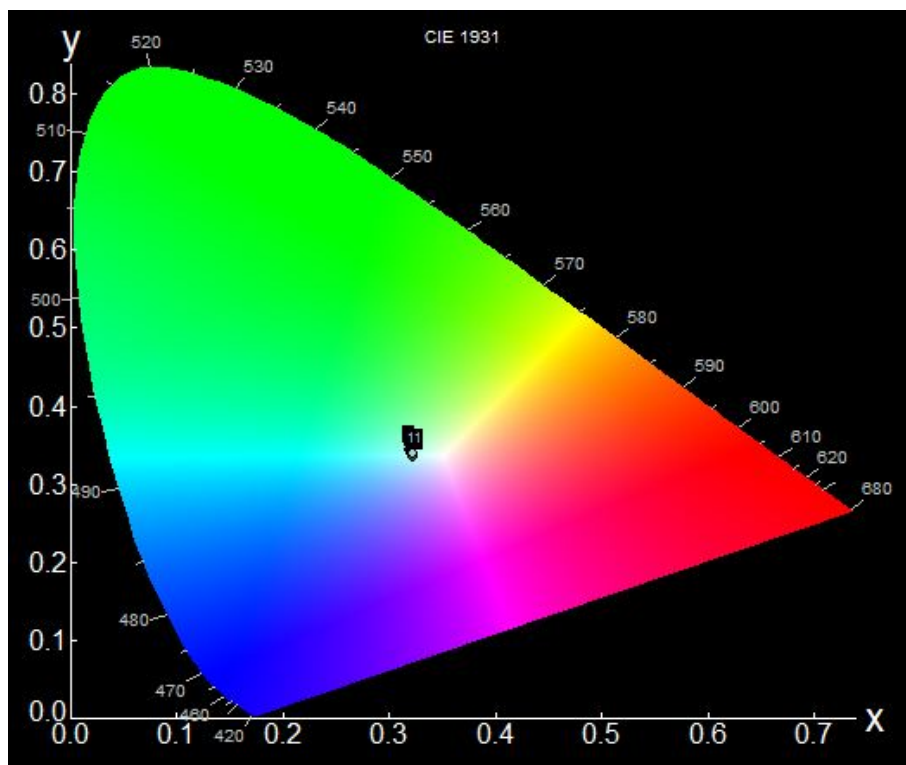


Figure S74. Shifts of the CIE of complex Dy_8L_4 under varying excitation wavelengths from 290 nm to 300 nm showing the location of the color-tunable chromaticity of emission image.

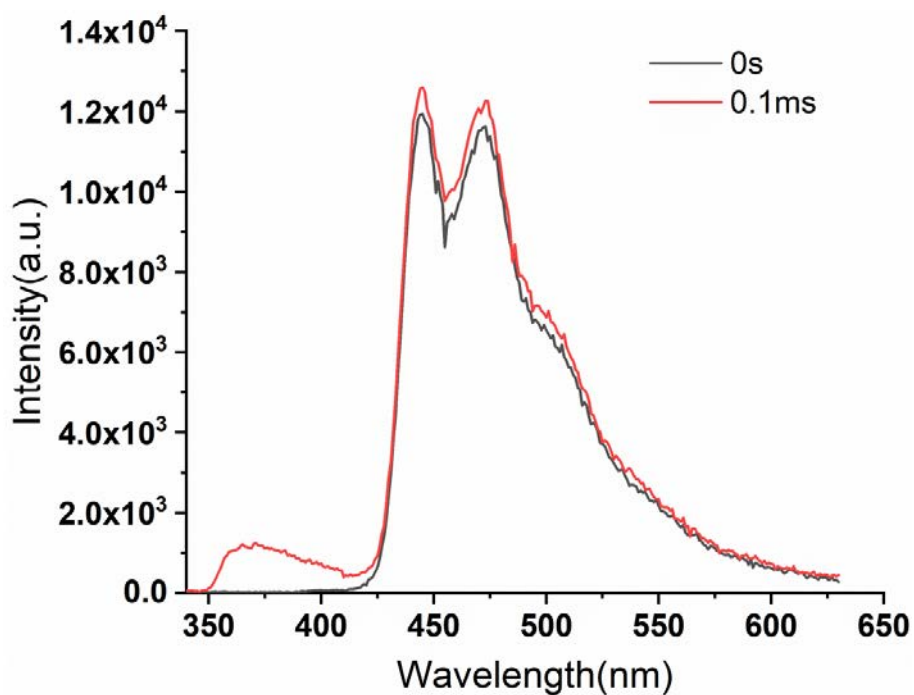


Figure S75. Phosphorescence spectra of Gd₈L₄ at 77 K ($c = 1 \times 10^{-5}$ M, CH₃CN).

Table S7. Summary of fluorescence properties of ligand L assemblies

LOPs	λ_{ex} (nm)	λ_{em} (nm)	Φ (%)
Tb ₈ L ₄	345nm	543nm	92.74%
Sm ₈ L ₄	348nm	595nm	0.88%
Dy ₈ L ₄	347nm	572nm	2.79%

Table S8. Summary of different modulation to WLE

LOPs	λ_{ex} (nm)	CIE
Dy ₈ L ₄	290	0.319,0.344
	291	0.321,0.343
	292	0.320,0.341
	293	0.321,0.339
	294	0.322,0.340
	295	0.323,0.339
	296	0.323,0.337
	297	0.323,0.336
	298	0.322,0.334
	299	0.322,0.335
	300	0.322,0.339

7. Reference

1. F. Yin, J. Yang, L.-P. Zhou, X. Meng, C.-B. Tian and Q.-F. Sun, 54 K Spin Transition Temperature Shift in a Fe₆L₄ Octahedral Cage Induced by Optimal Fitted Multiple Guests, *J. Am. Chem. Soc.* 2024, **146**, 7811-7821.
2. O. V. Dolomanov, L. J. Bourhis, R. J. Gildea, J. A. K. Howard and H. Puschmann, OLEX2: a complete structure solution, refinement and analysis program, *J. Appl. Cryst.* 2009, **42**, 339-341.
3. Spek, A. L. Single-Crystal Structure Validation with the Program PLATON, *J. Appl. Crystallogr.* 2003, **36**, 7.
4. J. B. Maglic and R. Lavendomme, MoloVol: an easy-to-use program for analyzing cavities, volumes and surface areas of chemical structures, *J. Appl. Crystallogr.*, 2022, **55**, 1033-1044.